12/7/89 CDF/PUB/ELECTROWEAK/PUBLIC/1089

Search for a light Higgs Boson produced in association with an Intermediate Vector Boson at the Fermilab Proton-Antiproton Collider

E. Buckley, S. Geer, E. Pare, C. Wendt

1. Introduction

We have searched for a light Standard Model Higgs boson ($2m_\mu < m_H < 2m_\rho$) produced in association with a W or Z boson (fig. 1) at the Fermilab Proton-Antiproton Collider operating at a center-of-mass energy of 1.8 TeV. The method follows that of ref. [1]. The predicted fraction of W and Z events containing an associated Higgs boson is shown as a function of m_H in fig. 2 [2]. A light Higgs boson would be produced in about 1% of all W and Z events. Higgs bosons with mass above the e^+e^- threshold and below the $\rho^+\rho^-$ threshold will decay to a charged track pair (e^+e^-, $\mu^+\mu^-$, $\pi^+\pi^-$, or K^+K^-) with a branching fraction [3,4] of greater than 50% (fig. 3). The predicted lifetime of the Higgs boson decreases rapidly with increasing m_H in the neighborhood of the $\mu^+\mu^-$ threshold. Above the $\mu^+\mu^-$ threshold the lifetime is short and the charged track pair will be associated to the vertex (fig. 4). The Higgs boson is expected to be produced at relatively high transverse momentum (p_T), resulting in a high-p_T charged track pair (fig. 5). We have therefore searched for a resonance in the mass distribution of isolated high-p_T charged-track-pairs in the CDF W and Z event samples.

2. Data Selection

Our W and Z selection criteria, data samples, and estimated backgrounds are listed in tables 1 and 2 and the associated uncorrected Z mass and W transverse mass distributions are shown in fig. 6. There are a total of 5224 W decays and 480 Z decays after background subtraction. The backgrounds have been evaluated as follows :

(i) Central $W \rightarrow e\nu$; The contribution to the $W \rightarrow e\nu$ sample from processes that do not produce genuinely isolated electrons (e.g. heavy flavour production, jet fluctuations) has been evaluated by comparing the electron isolation and E/p distributions for the $W \rightarrow e\nu$ electrons with a control sample of high-p_T tracks in large missing-E_T events where the tracks fail the EM fraction requirement. The resulting background has been estimated to be 3.5 ± 2.0 % [6].

(ii) Plug $W \rightarrow e\nu$; The background from non-W related processes has been estimated to be $6.2 \pm 2.7\%$ [7] by studying the distribution of missing-E_T significance (missing-$E_T/\Sigma E_T$) for the inclusive plug electron sample and extrapolating the rapidly decreasing low missing-E_T background above the cut (missing-$E_T/\Sigma E_T > 2.4$).

(iii) $W \rightarrow \mu\nu$; A comparison of the missing-E_T distributions associated with perfectly isolated and less than perfectly isolated muons in W candidate events suggests that in the region $20 < p_T^{\mu} < 40$ GeV/c the contribution to the sample from processes which do not in general produce an isolated muon (e.g. heavy flavour production and semileptonic decay) is negligible [8]. The high-missing-E_T tail is less well studied. We will estimate the extreme limits of the background based on the assumptions that either all of the tail ($m_T^{\mu\nu} > 100$ GeV/c^2) is background or all of the tail is signal. The resulting background estimate is $2.2 \pm 2.2\%$.

(iv) Z; The background in the Z samples is estimated to be $3 \pm 2\%$.

3. Pair Selection

To search for isolated high-p_T track pairs in the W and Z events, after excluding the W/Z decay lepton track(s), we consider CTC tracks passing the following cuts:

$p_T > 500$ MeV/c

$|\eta_{detector}| < 1.2$

$N_{hits} > 45$

$|z_0 - z_{vertex}| < 5$ cm

impact parameter $d < 1$ cm

3-D track (r-ϕ-z fit)

The tracks were reconstructed using 5.1 production with no beam-constraint. We consider oppositely charged track pairs where, to reduce combinatorics, both tracks are separated in η-ϕ space by no more than $\Delta R = 1.0$ ($\Delta R \equiv \sqrt{\Delta\eta^2+\Delta\phi^2}$). The typical separation of the daughter tracks from Higgs boson decay is $\Delta R \approx 0.2$ for $m_H = 1$ GeV/c^2, and the expected loss outside a cone of $\Delta R=1.0$ is small (see table 5). To reduce CTC edge effects, we further require that the axis of the track pair is within the pseudorapidity interval $|\eta_{detector}| < 1.0$. In addition the pair axis must be separated from the W/Z decay leptons by $\Delta R > 0.4$. There are a total of 27819 pairs passing these cuts.

The main source of high-p_T track pairs in W and Z events arises from initial-state bremsstrahlung jets produced in association with the weak bosons. These track pairs will not in general be isolated. We therefore require that our track pairs be isolated in a cone with size typical of these bremsstrahlung jets $\Delta R = 0.6$ (fig. 7). We first consider isolation

of the track pair in the CTC. To determine the value of the isolation cut and the associated loss of genuinely isolated track pairs we have randomly thrown cones in the central $W \rightarrow e\nu$ event sample and calculated the sum of the CTC track p_Ts within this cone:

$$I_{CTC} \equiv \sum_{\Delta R=0.6} p_T.$$

The cone axis has been distributed uniformly in $\eta_{detector}$ ($|\eta_{detector}| < 1.0$) and ϕ, and the W decay electron has been excluded from the sum. The resulting distribution is shown in fig. 8a. We require that $I_{CTC} < 1.2$ GeV/c. The loss of genuinely isolated pairs associated with this cut is 19.4±0.4% (fig. 8b). The uncertainty on the loss is statistical and arises from the limited number of independent cones that can be thrown in the W sample (10 cones per W). In calculating the loss we have assumed that the direction of the Higgs boson is uncorrelated with the direction of any activity associated with the W production. If the Higgs boson direction in the transverse plane is collinear (anticollinear) with the hadronic system recoiling against the W boson we find that the loss of Higgs bosons would increase (decrease) by 10% (6%). A Monte Carlo calculation (see section 5) of the expected correlation between the directions of the Higgs boson and the jet activity associated with the W production shows that the two tend to be anticollinear (fig. 9). Thus our calculated loss of genuinely isolated track pairs is slightly over-estimated.

We now consider isolation of the track pair in the calorimeter. We wish to construct the sum of energy depositions within our isolation cone $\Delta R = 0.6$ after excluding the energy associated with the track pair. To identify the energy depositions associated with the track pair the two tracks have been extrapolated to the mid-plane (in depth) of the calorimeters. Electromagnetic (hadronic) calorimeter cells which are within subcones of radius $\Delta R = 0.1$ (0.3) centered on the track impact positions have not been included in the sum. The subcone radii have been chosen so that the expected loss of energy from a showering pion outside of the subcones is negligible. We require that the resulting isolation variable

$$I_{CAL} \equiv \sum_{\Delta R=0.6} E_T \; - \sum_{SUBCONES} E_T$$

is less than 3.2 GeV. To determine the loss of genuinely isolated track pairs associated with this cut we have thrown cones $\Delta R = 0.6$ randomly in the central $W \rightarrow e\nu$ event sample, and for those cones passing the $I_{CTC} < 1.2$ GeV/c requirement we have calculated I_{CAL} where the directions of the subcones have been generated randomly within the isolation cone $\Delta R = 0.6$. The resulting distribution of I_{CAL} is shown in fig. 10a . The loss of genuinely isolated pairs with $I_{CAL} > 3.2$ GeV is 5.0± 0.2 ± 0.2% (fig. 10b). The second uncertainty is the systematic error associated with the uncertainty on the way the generated

subcones should be distributed within the isolation cone. We observe 7973 isolated track pairs passing these cuts.

4. Results

In fig. 11 the transverse momentum is shown for the positive (p_T^+) versus negative (p_T^-) tracks associated with the pair. There is a large accumulation of pairs with small values of p_T^+ and p_T^-. The mass distribution for the pairs (assuming the tracks are pions) is shown in fig. 12. No obvious narrow structure above background is observed. We believe that the observed background is associated with initial state bremsstrahlung jets fluctuating to fake an isolated track pair. We have repeated the analysis using a sample of 6549 multijet events (table 3), requiring at most one of the two highest-p_T jets to be in the central calorimeter, and that both tracks associated with the pair are separated from the jet axes by $\Delta R > 1.0$. We find 8320 pairs satisfying our selection cuts. The resulting p_T^+ versus p_T^- and pair mass distributions are shown in figs. 13 and 14. As expected, these distributions are qualitatively similar to the corresponding pair distributions associated with the W and Z sample. We note that the mean number of pairs for the IVB sample and the multijet sample are 1.40 ± 0.012 and 1.27 ± 0.01 respectively. As expected, these rates are similar but not identical.

To further reduce the background we consider pairs satisfying the additional cuts :

$$p_T^R \equiv \sqrt{(p_T^+)^2 + (p_T^-)^2} > 5 \text{ GeV/c}$$
$$|\cos\theta| < 0.9.$$

where the angle θ is the angle of the outgoing tracks with respect to the pair direction in the pair rest frame. The $\cos\theta$ distribution of the tracks (assumed to be pions) is shown before the application of the cut at $|\cos\theta| = 0.9$ in fig. 15. This distribution peaks at large $\cos\theta$, corresponding to asymmetric track pairs (p_T^+ very different from p_T^-).

We are left with 56 pairs that satisfy these requirements. The characteristics of the pairs in the mass region $m < 1.5$ GeV/c^2 are listed in table 4. To obtain the best pair masses for this final sample of track-pairs we have applied the beam constraint and refitted the tracks. The resulting pair mass distribution is shown in fig. 16a in the mass interval $m < 1.5$ GeV/c^2 and in fig. 16b for the mass interval $1.5 < m < 3$ GeV/c^2. We have assumed that the tracks are pions. In fig. 16c is shown the pair mass distribution in the mass interval $2m_K > m > 2m_\rho$ where both the $\pi^+\pi^-$ and the K^+K^- hypotheses are considered for the tracks. For the majority of the track pairs the energy deposited in the calorimeter cells is too large to be consistent with an isolated $\mu^+\mu^-$ assignment to the pair. The energy deposited in the cells associated with the pair is shown in fig. 17a for pairs where the

separation in ΔR_{+-} of the extrapolated tracks at the front face of the hadron calorimeter is less than 0.3, and in fig. 17b for $\Delta R_{+-} > 0.3$. For pairs whose $\Delta R_{+-} < 0.3$ we have rejected the $\mu^+\mu^-$ hypothesis for the tracks if the combined energy deposited in the electromagnetic calorimeter $E_{EM}^1+E_{EM}^2$ is greater than 1.5 GeV or the combined energy in the hadron calorimeter $E_{HAD}^1+E_{HAD}^2$ is greater than 6 GeV. If the pair has $\Delta R_{+-} > 0.3$ then we reject the $\mu^+\mu^-$ hypothesis for the tracks if $MAX(E_{EM}^1,E_{EM}^2) > 1$ GeV or $MAX(E_{HAD}^1,E_{HAD}^2) > 4$ GeV. These numbers are based on experience from the $Z \rightarrow \mu^+\mu^-$ analysis and on a study of $J/\psi \rightarrow \mu^+\mu^-$ decays. In the Z analysis it was found that (looser) cuts of $E_{EM} < 2$ GeV and $E_{HAD} < 6$ GeV are 98% efficient for identifying muons of $p_T > 5$ GeV/c [5]. The distributions of E_{EM} and E_{HAD} are plotted in fig. 18 for muons from J/ψ decays, showing the tighter cuts used in the Higgs search. From this sample, the efficiency for identifying muon pairs has been calculated as $(91.4 \pm 2.5)\%$ for $\Delta R_{+-} > 0.3$ and $(92.0 \pm 2.3)\%$ for $\Delta R_{+-} < 0.3$. Five pairs in the mass region of interest, $2m_\mu < m < 2m_\rho$, are consistent with a $\mu^+\mu^-$ assignment. These ambiguous pairs are indicated in table 4 and fig. 16a.

The pair mass distribution is featureless in the region of interest ($2m_\mu < m < 2m_\rho$). In order to proceed further we need to know (i) the pair mass resolution, and (ii) the expected number of Higgs bosons that would survive our selection cuts.

4. Mass Resolution

To understand the relationship between the real pair-mass resolution and the value computed from the track covariance matrices stored in the CTCS banks, we have studied the calculated and observed width of the $J/\psi \rightarrow \mu^+\mu^-$ mass peak. We note that the calculated resolution has roughly equal contributions from the error on cot θ and from the error on the phi-curvature (fig. 19) enabling us to study both of these contributions. The contribution from $\delta\cot\theta$ is small when the opening angle is predominantly $\Delta\phi$ and large when it is predominantly $\Delta\theta$. We divided the J/ψ sample into two classes of events corresponding to those decays for which the contribution to the mass resolution from $\delta\cot\theta$ is the dominant contribution (larger than the remaining contribution to the uncertainty) and those decays where it is not the dominant contribution. The mass distributions for these two classes of decays are shown in figs. 20a and 20b. From the widths of these distributions we conclude that to get the mass error correct we must multiply both the cot θ and phi-curvature contributions calculated from the covariance matrices by 1.5. This factor is believed to reflect the contributions from bad hits and imperfect pattern recognition (things that are hard to calculate analytically). Including these factors of 1.5 in the calculation the deviation from the central mass for the J/ψ decays divided by the calculated mass-resolution is shown in

figs. 20c and 20d for the two classes of decays. Both of these distributions are consistent with unit width Gaussians. We conclude that the resolution is being calculated correctly to within ±20%.

The degradation of the curvature resolution compared to that given in the CTCS covariance matrix has also been observed in a study of calorimeter energy versus track p_T [9]. In addition, the resolutions for the different components of the CTC track measurements have been studied [10] by matching the two halves of cosmic ray tracks. That study suggested that only the phi measurement error required degradation, the curvature uncertainty being correct to within ±5%. The difference between the J/ψ results and the cosmic ray results may be attributed to the cleaner environment associated with cosmic ray events. The J/ψ results are more directly relevant as a calibration for the Higgs search, both because the real underlying events are taken correctly into account, and because the same beam constraint has been applied to both the J/ψ and Higgs analyses.

The mass resolutions for the track pairs surviving the Higgs boson search selection have been computed from the track covariance matrices including the calibration factors of 1.5 extracted from the J/ψ analysis. The distribution of mass-uncertainties for the pairs is shown in fig. 21. The average pair-mass resolution for pairs with mass $2m_\mu < m < 2m_\rho$ is 6.9 MeV/c^2. The dominant contribution comes from the opening angle measurement, in particular its polar angle component. The uncertainty in cot θ is typically ±0.0027 compared to ±0.0003 for φ. The curvature error is typically $\sigma(p_T)/p_T^2 = 0.0011$ GeV^{-1}.

5. Monte Carlo Predictions

To simulate Higgs production in association with W and Z bosons produced in proton-antiproton collisions at $\sqrt{s}$ = 1.8 TeV we have used the lowest order matrix elements for the processes shown in fig. 1. The spin 0 Higgs boson has been forced to decay with the branching fractions shown in fig. 3. We are interested in the fraction of W and Z events that contain a Higgs boson passing our selection cuts. Thus we have also calculated inclusive W production at $\sqrt{s}$ = 1.8 TeV. Our Monte Carlo calculations have been done by modifying PYTHIA to include the processes of fig. 1, setting m_W=80 GeV/c^2, m_Z = 91 GeV/c^2, $\sin^2\theta_W$ = 0.227, m_{top} = 80 GeV/c^2, and using the EHLQ 1 structure functions.

The Monte Carlo generated events have then been passed through the detector simulation program CDFSIM, where the vertex position has been smeared in z to correspond to the observed distribution in the 1988/89 run. Fig. 2 shows the predicted fraction of W and Z events containing a Higgs boson as a function of Higgs mass before any cuts. This fraction is of order 1%. The theoretical uncertainty on this prediction is very small since the contribution from higher-order (purely weak) processes is negligible,

and the uncertainty in the absolute production rates due to structure functions and higher-order (strong) processes largely cancel in the ratio $\sigma(W+H)/\sigma(W)$. We note that our predictions for $\sigma(W+H)/\sigma(W)$ are in agreement with a previous calculation done for Higgs production at $\sqrt{s}$ = 630 GeV [1] using the Eurojet Monte Carlo. Note that $\sigma(W+H)/\sigma(W)$ is expected to be only weakly dependent on $\sqrt{s}$.

The expected number of Higgs bosons passing our selection cuts is shown as a function of Higgs mass in table 5. In the mass range of interest the number varies only slowly with mass. The loss of Higgs bosons due to the isolation cuts has been taken from the calculation described in section 2 in which random cones have been thrown in real W $\rightarrow e\nu$ events. We have also included a factor of 0.99 to allow for some inefficiency in the track reconstruction. Since we are looking for isolated, relatively high-p_T track pairs within $|\eta_{detector}| < 1.2$ we expect the real tracking efficiency to be better than this. The predicted p_T^+ versus p_T^- distributions and the cos θ distributions are shown as a function of Higgs boson mass in figures 22 and 23, which can be compared with the corresponding plots for the data (figs. 11 and 15 respectively). Note that Higgs boson decays surviving our selection cuts are associated with a flatter cos θ distribution and harder p_T^+ and p_T^- distributions than those observed in the data.

6. List of Systematic Uncertainties on the Predictions

Following is a list of systematic errors on the predicted number of Higgs bosons that survive our cuts:

(i) W and Z backgrounds: The total number of non-W related background events in the W sample is 213 ± 70 events, corresponding to an uncertainty of ± 1.4% on the final predicted number of Higgs bosons surviving our cuts. The corresponding background in the Z data samples is 15 ± 8 events, an uncertainty of ± 1.4%. The combined uncertainty on the W and Z data samples is 1.3%.

(ii) Fraction of W and Z bosons with associated Higgs boson production: Higher order weak corrections to the diagrams shown in fig. 1 are expected to be negligible. We have varied the W and Z masses, and $\sin^2\theta_W$ in the Monte Carlo within one standard deviation of the world average values, and found that the predicted fraction of W and Z events containing Higgs bosons changes by no more than ± 1.6%.

(iii) Higgs boson decay branching fractions: In the mass interval $2m_p < m_H < 2m_K$ the Higgs boson will decay into $\mu^+\mu^-$, $\pi^+\pi^-$, or $\pi^0\pi^0$. The expected branching fraction of the Higgs boson into the pion modes calculated in ref. [4] is about 0.7 in the mass region of interest. To avoid any model dependence in our limits on m_H we make the most pesimistic

assumption, namely that the Higgs boson decays exclusively into the pion decay modes, in which case one-third of the Higgs boson decays will be lost in the $\pi^0\pi^0$ mode.

(iv) Isolation: We add the statistical uncertainties on the loss of isolated track pairs due to our isolation criteria in the CTC and calorimeters in quadrature, and add the result linearly to the systematic uncertainty on the loss due to the calorimeter isolation requirement. The resulting overall uncertainty is $\pm$ 0.6%.

(v) Higgs-boson-p_T (p_T^H) and structure functions: We are selecting relatively high-p_T track-pairs. Our predictions are therefore sensitive to the p_T^H distribution. We have checked that PYTHIA gives a good description of the observed p_T distribution for inclusive W production, after smearing the parton level electron energies by $15\%/\sqrt{E}$ and the neutrino energy by $0.7/\sqrt{30+p_T^W}$ [6] to allow for detector resolution (fig. 24). To evaluate the systematic uncertainty on the predictions due to the uncertainty on the p_T^H distribution we have reduced the component of p_T^H in PYTHIA associated with the incoming annihilating partons (after gluon radiation) by 20% , and found that the number of Higgs bosons predicted to survive our cuts decreases by no more than 3%. We therefore assign a systematic uncertainty of $\pm$3% to our predicted Higgs boson rate due to the uncertainty on the p_T^H distribution. We have also used alternative structure functions (EHLQ2 [11], DO1 [12], and DO2 [12]). In all cases the predicted Higgs boson rate is consistent within $\pm$1.8% with the EHLQ1 prediction.

To take account of all of these uncertainties we have reduced our predicted Higgs boson rate by one systematic standard deviation (3.7%), calculated by combining all of the above components in quadrature. The resulting theoretical floor is shown in table 5 and fig. 26.

7. Fitting and Limits

The 90% and 95% C.L. upper limits on the number of Higgs bosons contributing to the selected pair sample are shown as a function of m_H in fig. 26. This limit has been obtained by fitting the observed pair mass distribution in the region $2m_\mu < m_H < 2m_\rho$ by the method of maximum likelihood [13]. The parent distribution has been assumed to be described by a Higgs boson peak superimposed on a flat background. An extended likelihood method was used, allowing the signal and background contributions to vary independently (i.e. their sum was not constrained to the observed number of events). The fit takes account of the mass and mass resolution for each of the 32 observed pairs. This is done in the usual way by calculating the probability density at the position of each pair after smearing the theoretical prediction (delta function plus flat background) by the pair mass resolution function. The likelihood is then calculated by taking the product of the

probability densities for all the pairs. The fit has been made imposing the constraint that the number of Higgs bosons is non-negative. This physical bound has been applied using the Baysean method which is the method recommended and described in the 1988 particle data booklet (see also ref. [13]) In this method the integral of the probability density function over the physical region of parameter space ($n_H > 0$) is re-normalized to unity. The method is known to give "true" limits when the hypothetical theory is far from the physical bound and "conservative" limits when the theory approaches the bound ($n_H \sim 0$).

To check that the fitting program gives reasonable results we have generated 1000 Monte Carlo experiments for which there are n_H Higgs bosons, where n_H is distributed according to Poisson statistics with a mean of (a) 5 (far from the bound), and (b) 2 (close to the bound). The CDF sensitivity corresponds more closely to case (a). The Higgs boson mass was centered on 500 MeV/c^2, and smeared by the resolution function, which was taken to be a Gaussian with a width picked randomly for each generated pair from the mass errors asociated with the observed pairs in the data. Each generated experiment consists of n_H Higgs bosons plus a flat background, where the mass errors for the background pairs were also picked randomly from those associated with observed pairs in the data. The total number of pairs in each generated experiment was fixed to the observed number of 32. The generated experiments were then fit by the procedure described above. The resulting distribution of 68%, 90%, and 95% upper confidence limits found by the fitting program are shown in figs. 25a and 25b for the $\langle n_H \rangle = 5$ and 2 cases respectively. We note that:

(i) When $\langle n_H \rangle = 5$ the true hypothesis ($n_H = 5$) is accepted 68±2 % of the time at 68% C.L., 89±1 % of the time at 90% C.L., and 93.4±0.8 % of the time at 95% C.L. Thus the program gives the correct results.

(ii) When $\langle n_H \rangle = 2$ the true hypothesis ($n_H = 2$) is accepted 75±5 % of the time at 68% C.L., 97.6±0.6 % of the time at 90% C.L., and >99 % of the time at 95% C.L. Thus, as expected, close to the physical bound the procedure gives a conservative result.

We have considered the possibility that the background shape is not flat. Clearly a flat distribution does give an excellent description of the pair mass distribution. Fitting the background shape $b = \alpha m + c$, where both the slope parameter α and the total number of pairs in the distribution N (and hence the offset c) are allowed to vary, we find that the fit gives $N = 32^{+6}_{-5}$ pairs and $\alpha = (0.0 \pm 2.0) \times 10^{-5}$ pairs/MeV^2. As expected α and N are highly correlated, this correlation has been taken into account. Varying the slope parameter α by ±1 standard deviations changes the predicted background density at the extreme edges of the mass plot by ~ 30%. Since the background contribution within one bin of mass resolution is 0.2 - 0.3 pairs, the overall effect of changing α by $=1\sigma$ is to change the limit curves by < 0.1 pairs.

The results of fitting the observed pair mass distribution are shown in fig. 26. To take account of the systematic uncertainty on the pair-mass resolution the uncertainty on each pair mass has been increased by 20%. This increase broadens the peaks in the C.L. curves but does not appreciably change their height. The fit results are insensitive to reasonable changes in the assumed background shape. We note that more than five pairs associated with Higgs boson production is excluded everywhere at 90% C.L. except in the neighborhood of 832 MeV/c^2 where a small accumulation of events, consistent with statistical fluctuations, effectively weakens the limit.

8. Conclusions

We have made the first search for a Higgs boson produced in association with a real or nearly real Intermediate Vector Boson. A light Standard Model Higgs boson is excluded at 95% C.L. in the region $2m_\mu < m_H < 2m_\pi$, and at 90% C.L. in the region $2m_\pi < m_H < 2m_K$ except in the neighborhood of 832 MeV/c^2 ($\pm$ 14 MeV/c^2) where there is a small accumulation of events, consistent with statistical fluctuations. Over most of the mass interval a light Standard Model Higgs boson is also excluded at 95% C.L. There have been a number of previous searches for light Higgs bosons produced in pion[14], kaon[15], η'[16], B meson [17], and upsilon [18] decays. However, in the mass region $2m_\pi < m_H < 2m_K$ these previous results have required that the branching ratio for the Higgs boson to decay into $\mu^+\mu^-$ be significant. Our result is independent of this assumption [19].

REFERENCES

[1] 'Search for the Higgs boson: present status and future prospects for UA1', S. Geer, UA1 technical note UA1 TN 88-29 (1988), unpublished.

[2] J. Finjord, G. Giradi and P. Sorba, Phys. Lett. **89B** (1979) 99.

[3] J. Ellis, K. Gaillard and D.V. Nanopoulos, Nucl. Phys. **B106** (1976) 292.

[4] M.B. Voloshin, ITEP 85-153.

[5] F. Abe et al. (CDF Collab.) Phys. Rev. Lett. **63**(1989)720.

[6] Private communication, Paul Tipton, and CDF Note 1048.

[7] Private communication, Satoru Ogawa.

[8] Private communication, Tom Westhusing

[9] Private communication, Peter Berge.

[10] 'CTC tracking studies with cosmic rays', A. Gauthier, CDF note 965.

[11] E. Eichten et al., Rev. Mod. Phys. **56**(1984)579, and Erratum **58**(1986)1065.

[12] D. Duke and J. F. Owens, Phys. Rev. **D30**(1984)49.

[13] See for example L. Lyons, "Statistics for nuclear and particle physicists", Cambridge University Press, 1989.

[14] S. Egli et al., preprint PSI-PR-89-02(1989).

[15] T. Yamazaki et al., Phys. Rev. Lett. **52**(1984)1089.
N. Baker et al., Phys. Rev. Lett. **59**(1987)2832.
A. S. Carroll et al., Phys. Rev. Lett. **44**(1980)525.
E. Jastrzembski et al., BNL experiment E780, preprint BNL-41507, July 1988.
L. K. Gibbons et al., FNAL experiment E731, Phys. Rev. Lett. **61**(1988)2661.
P. Bloch et al., Phys. Lett. **56B**(1975)201.
R. J. Cence et al., Phys. Rev. **D10**(1974)776.
V. Bisi et al., Phys. Lett. **25B**(1967)572.
M. Mannelli, preprint BNL-41506, presented at the XXIII Rencontre de Moriond, March 1988.
Y. Asano et al., Phys. Lett. **113B**(1982)195, **107B**(1981)159.

[16] V. A. Viktorov et al., Sov. J. Phys. **33**(1981)822; R. I. Dzhelyadin, Phys. Lett. **105B**(1981)239.

[17] H. J. Behrend et al., Z. Physik **C10**(1983)291.
M. Althoff et al., Z. Physik **C22**(1984)218.
P. Avery et al., Phys. Rev Lett. **53**(1984)1309.
M. S. Alam et al. (CLEO Collab.) preprint CLNS-89/888(1989).

H. Albrecht et al., Phys. Lett. **B199**(1987)451.

A. Snyder et a. (MARK II Collab.) preprint SLAC-PUB-4986 (1989).

[18] P. Franzini et al., Phys. Rev. **D35**(1987)2883.

M. Narain et al., XXIV Int. Conf. on High Energy Physics, Munich, August 4-10, 1988.

H. Albrecht et al.(ARGUS Collab.), XXIV Int. Conf. on High Energy Physics, Munich, August 4-10, 1988.

[19] Except in the small region between the $\pi^0\pi^0$ and $\pi^+\pi^-$ thresholds where we have no limit if the branching ratio for the Higgs boson to decay into $\mu^+\mu^-$ is less than 0.33.

Table 1: Summary of W and Z data sets including cuts

Sample	Files	Selection cuts
$W \rightarrow e\nu$	WCENTRAL.EVT	$E_T^e > 20$ GeV
(central)	WCENTRAL_II.EVT	$E_T^m > 20$ GeV
		$m_T > 40$ GeV/c^2
		E/P < 1.5
		LSHR < 0.2
		Track-strip $\Delta(r\text{-}\phi) < 1.5$ cm
		$\Delta z < 3$ cm
		Border tower < 2 GeV
		Strip χ^2 < 10
		Had/Em Intercept=0.053
		Slope = 0.043
		Number of 3D tracks ≥ 1
$W \rightarrow e\nu$	PLUG_W1.CAND	$E_T^e > 20$ GeV
(plug)	PLUG_W2.CAND	$E_T^m > 20$ GeV
	PLUG_W3.CAND	$m_T > 40$ GeV/c^2
	PLUG_W4.CAND	Had/Em Intercept=0.053
	PLUG_W5.CAND	Slope = 0.043
	PLUG_W6.CAND	VTPC hit occupancy > 0.5
		χ^2 (Pad 3 × 3) < 10
$W \rightarrow \mu\nu$	WMU_MINI.CAND	$p_T^\mu > 20$ GeV/c
	WMU_MINI_CExxxx.CAND	$E_T^m > 20$ GeV
	where xxxx ≡ EMS03	$m_T > 40$ GeV/c^2
	tape number	$E_{EM} < 2$ GeV
		$E_{HAD} < 6$ GeV
		Impact parameter < 0.25 cm
		Energy in cone of $\Delta R = 0.4$
		including muon < 6.5 GeV
		$E_{EM} + E_{HAD} > 0$
		Require a muon-stub match to
		a CTC track within 10 cm
		$N_{hits} > 60$ for μ track
		Number of 3D tracks ≥ 1

		Back-to-back cut to remove cosmic rays
$Z \rightarrow e^+e^-$	WC_ZS.EVT WC_ZS_II.EVT	Central electron — all cuts for $W \rightarrow e\nu$ Plug/Forward electrons $E_T^e > 15$ GeV Had/Em Intercept=0.053 Slope = 0.043 $120 > m_Z > 65$ GeV/c^2
$Z \rightarrow \mu^+\mu^-$	ZMUON_ALL.CLEANER	$p_T^\mu > 20$ GeV/c $E_{EM} < 2$ GeV $E_{HAD} < 6$ GeV x-matching < 10 cm $N_{hits} > 60$ for m track $\lvert\eta_{detector}\rvert < 1.2$ for CMIO Back-to-back cut to remove cosmic rays No jet, $E_T > 15$ GeV within $\Delta R=0.4$ of muon Number of 3D tracks ≥ 1 $120 > m_Z > 65$ GeV/c^2

Table 1: W and Z data samples, luminosity, and estimated non-Intermediate-Vector-Boson associated backgrounds.

Sample	$\int L.dt$ (pb^{-1})	Events	Background
$W \rightarrow e\nu$ ($\lvert\eta_e\rvert < 1.1$)	4.4	3002	105 ± 60
$W \rightarrow e\nu$ ($\lvert\eta_e\rvert > 1.1$)	3.6	982	61 ± 26
$W \rightarrow \mu\nu$	4.4	1438	32 ± 32
$Z \rightarrow e^+e^-$	4.4	320	10 ± 6
$Z \rightarrow \mu^+\mu^-$	4.4	160	5 ± 3

Table 3: Multijet sample and selection cuts

Use all triggers on tapes from QCD02 stream.
Cuts:
Require than no more than one of the highest p_T jets are within $\lvert\eta\rvert < 1.2$
$E_T^m / \sqrt{E_T} < 2.0$
Tracks in pairs are required to be $\Delta R > 1.0$ from both of the highest p_T jet axes
Then apply track/pair selection cuts specified in text

Table 4: Characteristics of the 32 pairs in the mass region m < 1.5 GeV/c^2.

Run/Event	Type	p_T +	p_T -	p_T^2	ΔR	η	φ	cosθ*	Isolation I_{CTC}	Isolation I_{CAL}	Mass ee	Mass μμ	Mass ππ	Mass KK
		GeV/c	GeV/c	GeV/c					GeV/c	GeV	MeV/c^2			
											σ (MeV/c^2)			
16448/8244	W → eν	5.74	6.00	8.3	0.13	0.81	339	0.05	0.0	2.583	775	803	824	1257
											10.9	10.5	10.2	6.8
17200/3250	W → eν	1.25	9.54	9.62	0.17	0.69	244	0.83	0.452	1.228	574	658	715	1605
											5.2	4.9	4.9	6.7
17516/8772	W → eν	3.24	7.29	7.3	0.25	-0.32	237	0.42	1.064	0.810	1263	1284	1299	1663
											18.3	18.0	17.8	14.3
17865/763	W → eν	5.64	3.14	6.5	0.23	0.61	17	0.24	1.194	1.3545	985	1008	1025	1412
											13.7	13.4	13.2	9.5
18006/10151	W → eν	1.18	16.16	16.2	0.18	0.34	174	0.89	0.0	2.037	773	873	942	2035
											15.9	14.7	14.1	16.3
19114/48600*	W → eν	7.71	1.55	7.9	0.4	-0.01	202	0.69	0.746	0.661	1380	1408	1429	1904
											7.5	7.5	7.5	7.9
19153/35838*	W → eν	0.52	6.16	6.2	0.76	-0.47	67	0.89	0.46	0.997	1379	1440	1484	2281
											7.2	7.2	7.2	7.9
19238/52379*	W → eν	0.79	5.53	5.6	0.36	-0.48	135	0.82	0.0	0.033	714	786	837	1663
											7.3	6.8	6.6	5.7
19394/12152*	W → eν	5.79	0.52	5.8	0.7	0.58	67	0.83	0.289	0.517	1197	1247	1284	1990
											5.0	5.0	5.0	6.0
19932/13976	W → eν	5.91	4.66	7.5	0.27	0.04	333	0.12	0.0	1.82	1406	1422	1434	1723
											11.0	10.9	10.8	9.0
19943/11865*	W → eν	5.63	3.72	6.7	0.09	0.7	101	0.22	1.115	0.562	367	425	464	1072
											13.4	11.6	10.6	4.5
20060/111290	W → eν	7.26	2.61	7.7	0.2	0.33	338	0.49	0.0	0.0	883	915	938	1421
											6.2	6.0	5.9	4.9
20361/25112	W → eν	2.06	10.33	10.5	0.18	0.27	118	0.70	0.0	2.189	795	843	878	1532
											6.1	6.1	6.0	7.0
20394/22655	W → eν	4.77	2.31	5.3	0.38	0.35	173	0.33	0.0	0.0	1247	1266	1280	1624
											6.4	6.3	6.2	5.0
18858/10371	W → eν	3.40	4.37	5.5	0.15	0.82	215	0.09	0.0	1.618	533	573	602	1126
											10.9	10.2	9.7	5.1
16446/1635	W → eν	8.05	1.68	8.2	0.18	-0.9	110	0.68	0.70	2.928	631	683	721	1383
											7.6	7.1	6.7	4.8
17146/9678	W → eν	0.68	6.51	6.5	0.35	0.80	205	0.81	0.0	0.606	712	781	830	1648
											6.1	5.7	5.4	4.7
19629/84207	W → eν	1.33	5.76	5.9	0.11	0.10	284	0.78	1.094	1.643	237	358	428	1272
											9.6	6.4	5.4	2.9
20027/52553	W → eν	4.84	3.13	5.8	0.24	0.65	295	0.15	0.546	0.581	947	970	988	1377
											11.8	11.5	11.3	8.1
17074/5084	W → μν	3.91	3.48	5.2	0.37	1.13	186	0.002	0.0	1.141	1370	1386	1398	1689
											6.0	6.0	5.9	4.9
17253/3975	W → μν	9.50	3.62	10.2	0.14	0.03	102	0.47	1.121	3.001	837	870	894	1392
											3.0	3.0	3.1	4.1
19153/64112	W → μν	7.21	2.21	7.5	0.07	-0.4	313	0.70	0.0	0.941	282	374	431	1186
											9.1	7.0	6.2	3.9
19239/87886	W → μν	1.59	8.87	9.0	0.37	-0.59	18	0.70	0.0	0.315	1418	1447	1469	1963
											9.4	9.4	9.4	9.9
19367/6122	W → μν	11.58	3.17	12.0	0.16	0.58	152	0.62	0.729	2.832	1032	1065	1090	1619
											19.6	19.1	18.8	15.2
19428/28032	W → μν	6.59	2.68	7.1	0.31	-0.23	172	0.45	0.792	1.734	1235	1257	1273	1642
											9.3	9.2	9.1	7.5
20007/90463	W → μν	7.18	1.2	7.3	0.39	0.06	34	0.73	0.814	2.659	1142	1179	1207	1778
											9.9	9.7	9.5	8.0
16036/164	Z → e⁺e⁻	15.29	14.31	26.5	0.03	-0.46	110	0.04	0.979	1.621	449	496	529	1086
											14.2	12.9	12.1	5.9
17330/1136	Z → e⁺e⁻	0.94	5.03	5.1	0.35	-1.02	175	0.66	0.0	0.506	753	799	832	1460
											6.1	5.8	5.5	3.9
19116/17351	Z → e⁺e⁻	1.96	5.79	6.1	0.14	0.78	267	0.56	0.0	2.689	475	532	573	1226
											3.2	2.9	2.7	2.3
18031/12173	Z → e⁺e⁻	9.15	10.6	14.0	0.12	-0.75	52	0.11	0.0	1.854	1110	1130	1145	1487
											28.7	28.2	27.9	21.5
18038/11458	Z → e⁺e⁻	5.69	1.27	5.8	0.22	-0.14	172	0.70	0.0	1.748	589	649	691	1401
											9.6	8.7	8.2	5.0
16699/6903	Z → μ⁺μ⁻	13.01	2.7	13.3	0.03	-0.88	201	0.892	0.0	2.279	27	306	406	1431
											15.6	2.7	3.2	10.9

* Pairs for which both muon and pion assignments to the tracks are plausible.

Table 5: Predicted number of Higgs bosons surviving the selection criteria as a function of Higgs boson mass. The predictions are normalized to the total number of W and Z bosons in the CDF data samples. The predicted number of Higgs bosons surviving all cuts are given in the last three lines, which correspond to (i) the best estimate using the branching ratios of ref. [2], (ii) the best estimate reduced by one systematic standard deviation (see text), and (iii) further reduced to correspond to the most pessimistic scenario in which the Higgs boson decays only to the pion modes.

	m_H (MeV/c^2)								
Requirements	250	300	400	500	600	700	800	900	950
Before cuts	58.2	58.2	57.7	56.6	56.1	55.5	54.5	53.7	53.2
$H \rightarrow (\pi^+\pi^-$ or $\mu^+\mu^-)$	58.2	46.6	45.4	44.3	43.2	42.2	40.8	39.6	39.1
$\lvert\eta_{tracks}\rvert < 1.2$	39.5	31.3	29.7	28.4	27.4	26.4	25.1	24.1	23.5
$p_T > 0.5$ GeV/c	34.3	27.0	24.4	22.6	21.5	20.5	19.7	19.0	18.7
$\lvert\eta_{pair}\rvert < 1.0$	30.1	23.9	21.8	20.5	19.6	19.0	18.2	17.6	17.4
$\Delta R < 1.0$	30.0	23.7	21.6	20.1	19.1	18.3	17.2	16.4	16.0
ΔR(lepton,pair) > 0.4	28.2	22.3	20.2	18.8	18.0	17.2	16.1	15.3	14.9
$p_T^R > 5$ GeV/c	11.5	9.3	9.5	9.5	9.1	9.0	8.7	8.4	8.3
$\cos\theta < 0.9$	9.7	8.0	8.3	8.4	8.3	8.3	8.1	8.0	7.9
i) Isolation & tracking*	7.3	6.1	6.3	6.3	6.3	6.3	6.2	6.1	6.0
ii) Reduce by 1 σ_{SYS}	7.0	5.9	6.0	6.1	6.0	6.0	6.0	5.8	5.8
iii) Floor**	7.0	4.9	5.1	5.2	5.2	5.3	5.3	5.2	5.2

* Tracking × I_{CTC} efficiency × I_{CAL} efficiency ≡ (0.99 × 0.806 × 0.95) = 0.758

** The theoretical floor assumes that Br ($H^0 \rightarrow \pi\pi$) = 1

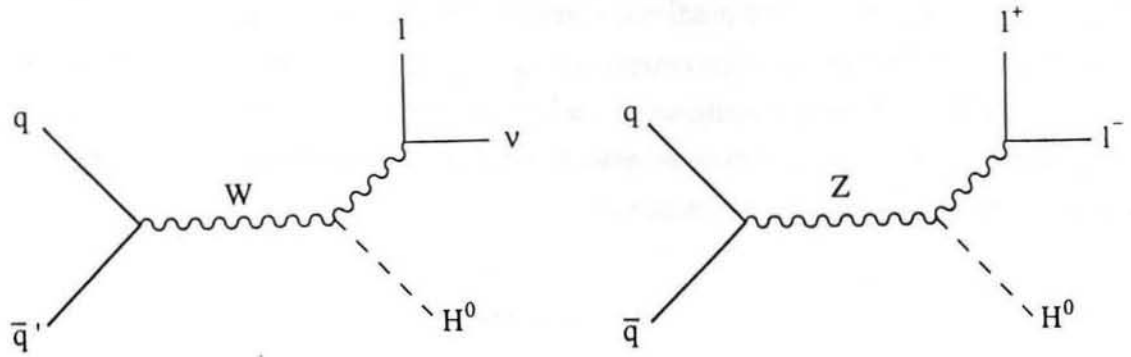

Fig. 1: Feynman diagrams for production of a Higgs boson in association with W and Z bosons.

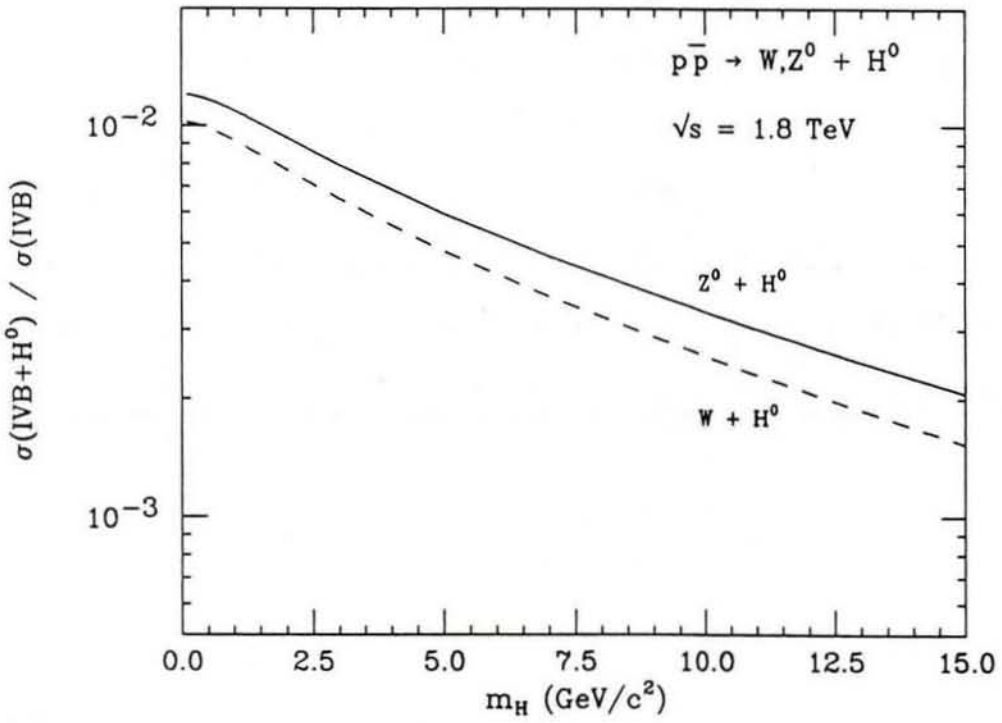

Fig. 2: The predicted fraction of W and Z, $\sigma(IVB+H)/\sigma(IVB)$, events containing an associated Higgs boson as a function of the Higgs mass m_H.

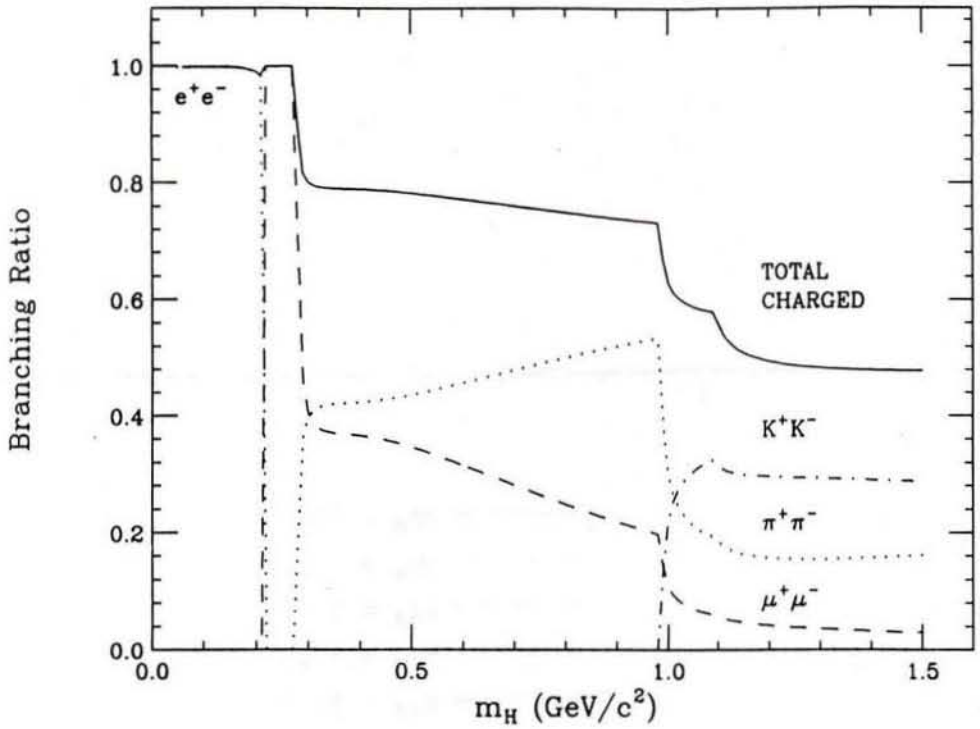

Fig. 3: Predicted branching fractions for Higgs boson decay as a function of the Higgs mass m_H.

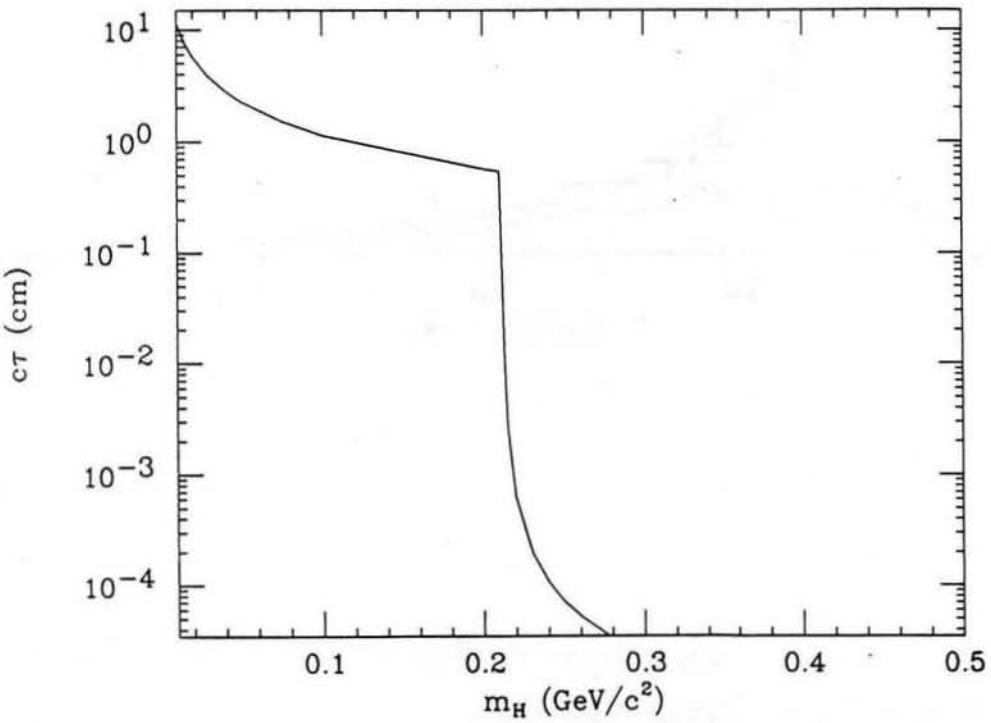

Fig. 4: The invariant decay length $c\tau$ as a function of the Higgs mass m_H.

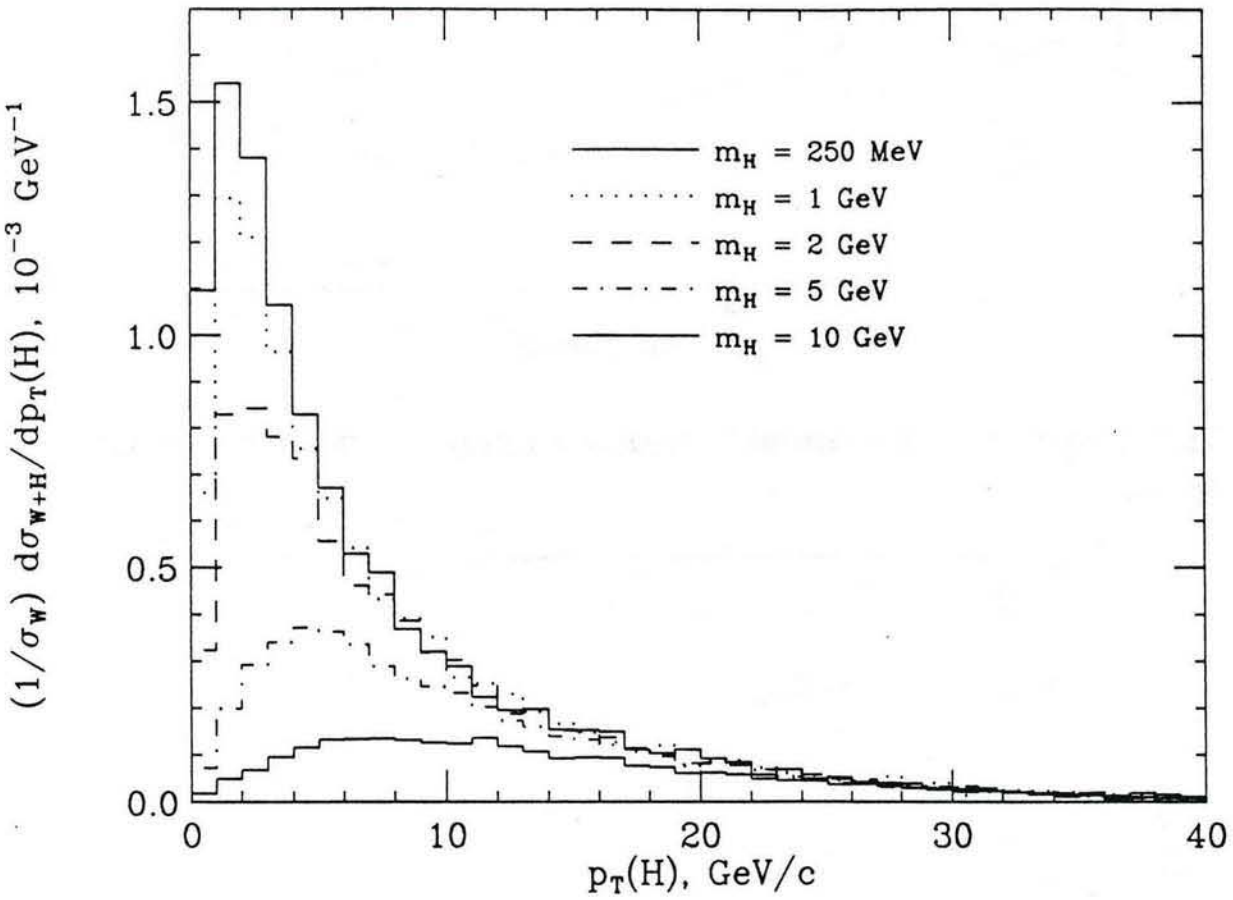

Fig. 5: The p_T spectrum $1/\sigma_W\ d\sigma_{W+H}/dp_T^H$ for the Higgs boson produced in association with W and Z bosons for five different Higgs masses.

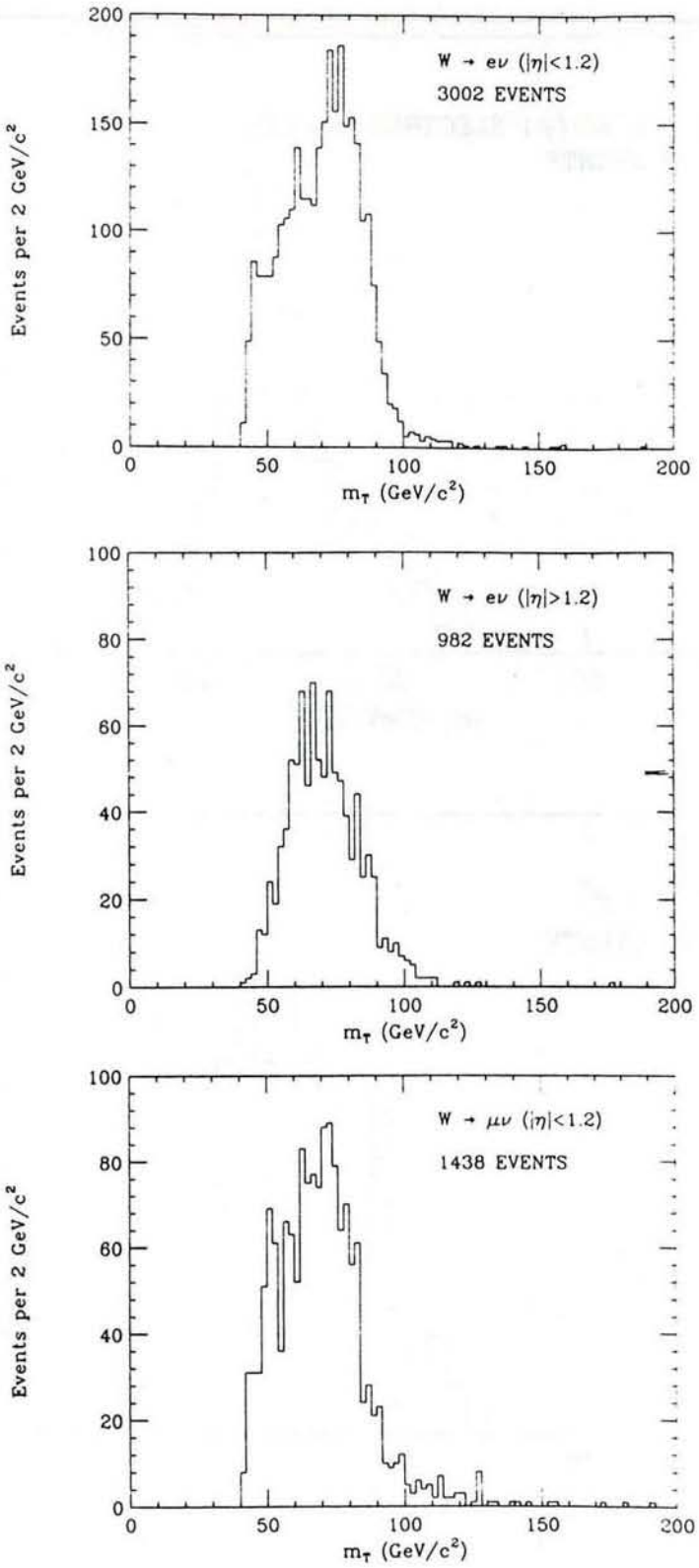

Fig. 6a: Uncorrected W transverse mass distributions for $W \rightarrow e\nu$ (central), $W \rightarrow e\nu$ (plug) and $W \rightarrow \mu\nu$.

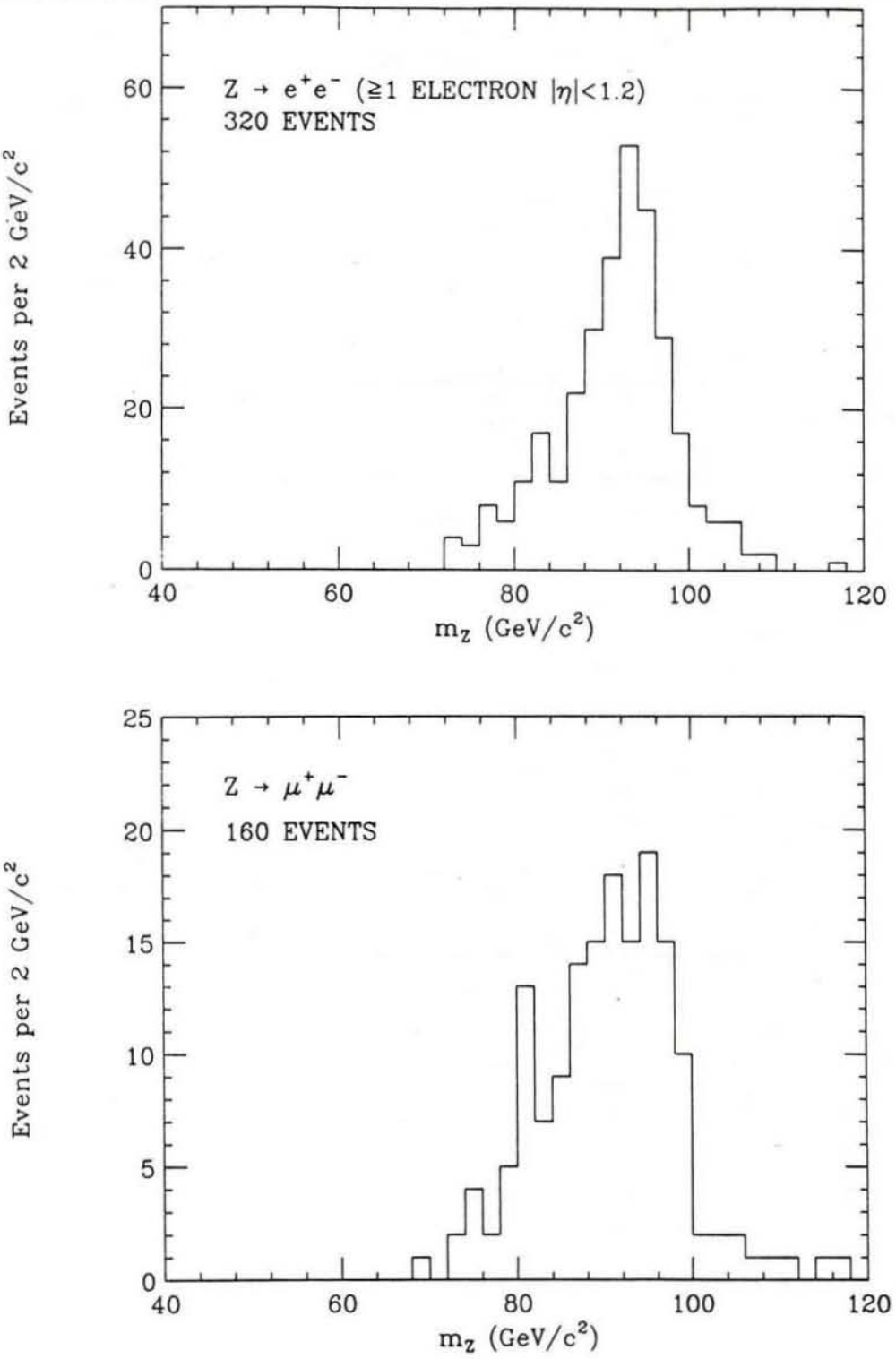

Fig. 6b: Uncorrected Z mass distributions for $Z \rightarrow e^+e^-$ and $Z \rightarrow \mu^+\mu^-$.

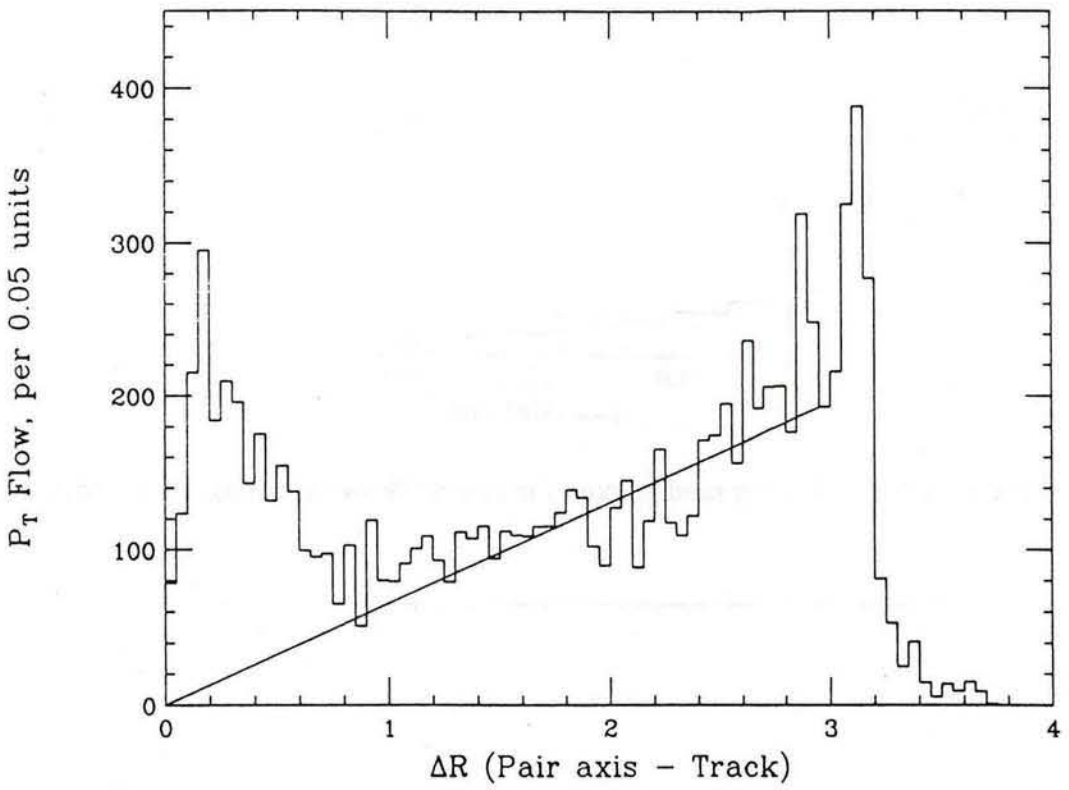

Fig. 7: Transverse momentum flow about the pair axis for multijet events. The pair tracks have been excluded. The curve reminds us that the area of an annulus at radius ΔR is proportional to ΔR.

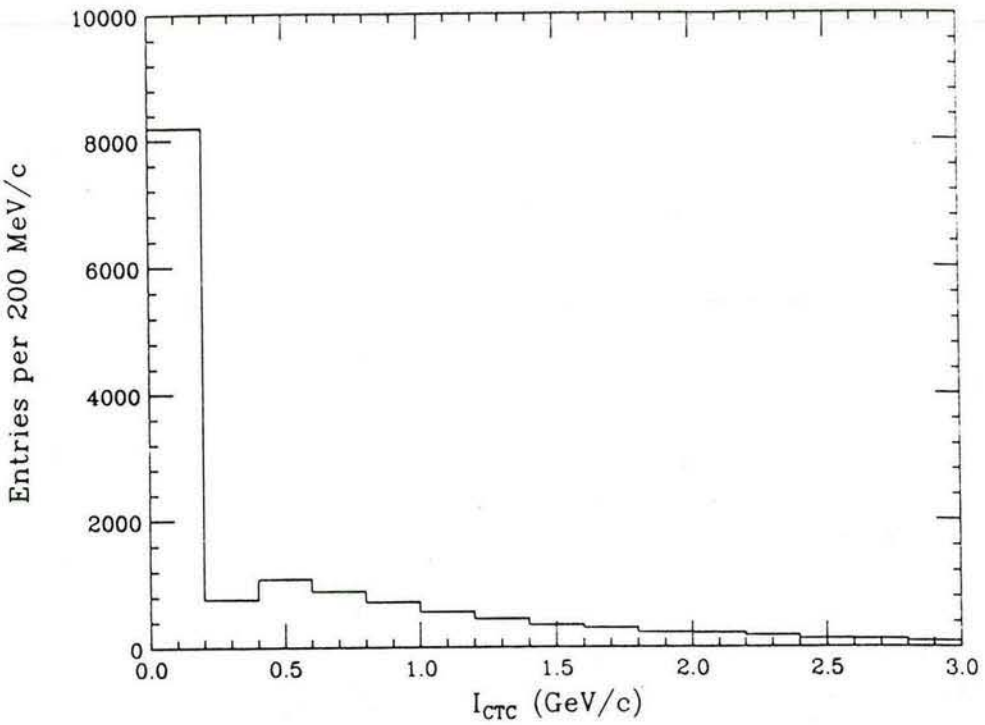

Fig. 8a: The distribution I_{CTC} for random cones in central $W \rightarrow e\nu$ events as described in section 2.

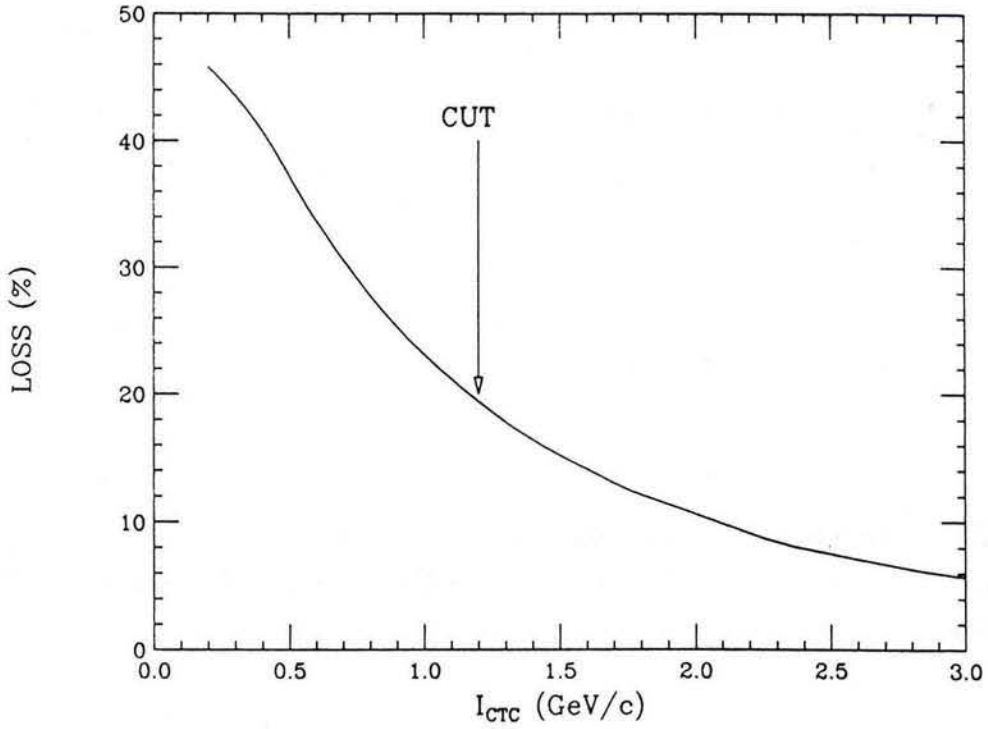

Fig. 8b: The loss of genuinely isolated track pairs as a function of the variable I_{CTC}.

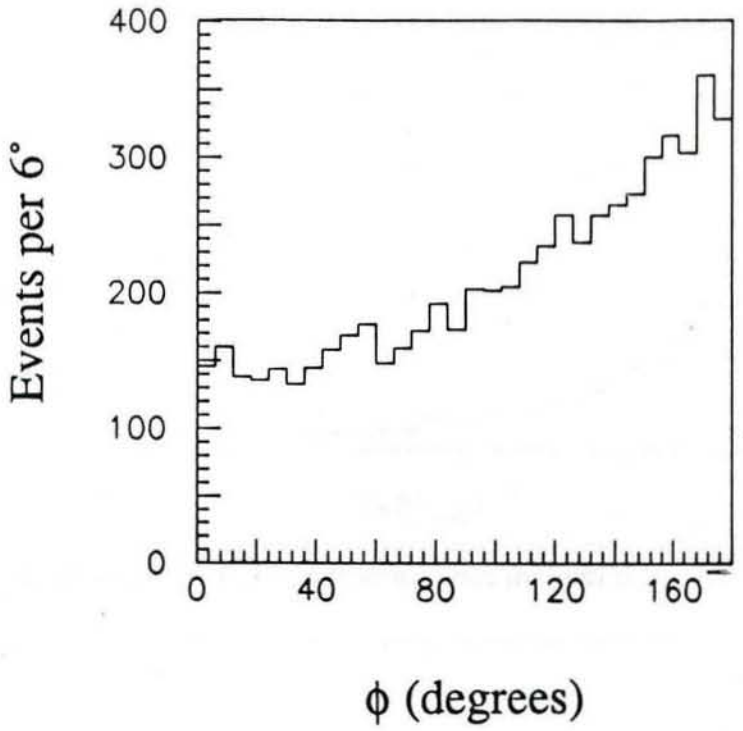

Fig 9: The angle ϕ between the transverse direction of hadronic system recoiling against the W boson and the transverse direction of the Higgs boson.

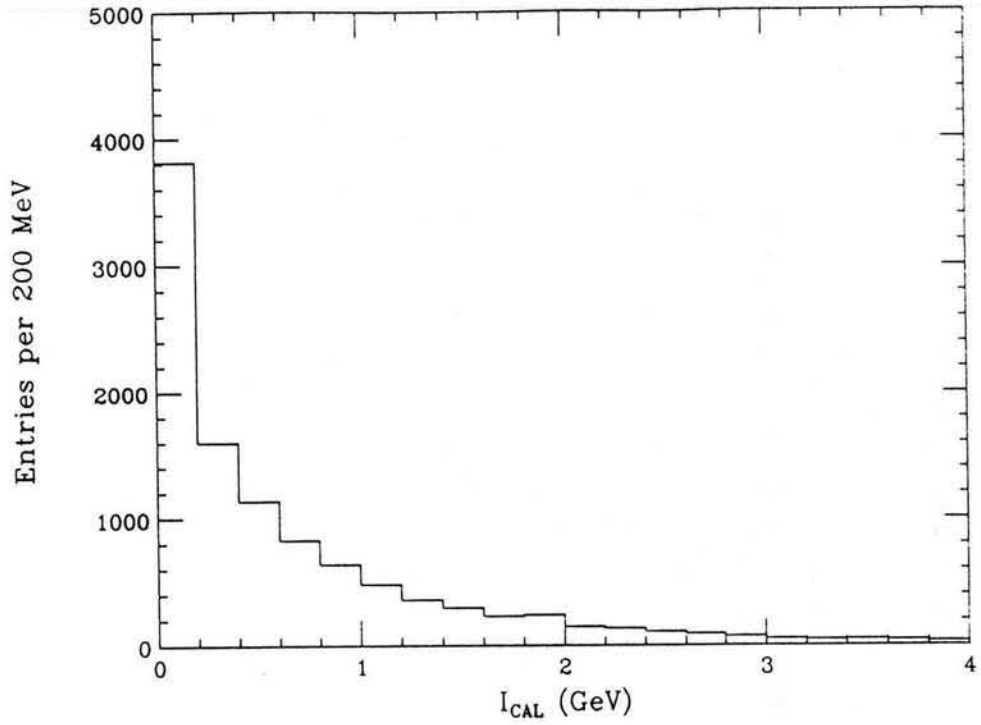

Fig. 10a: The distribution I_{CAL} for random cones in central $W \rightarrow e\nu$ events as described in section 2.

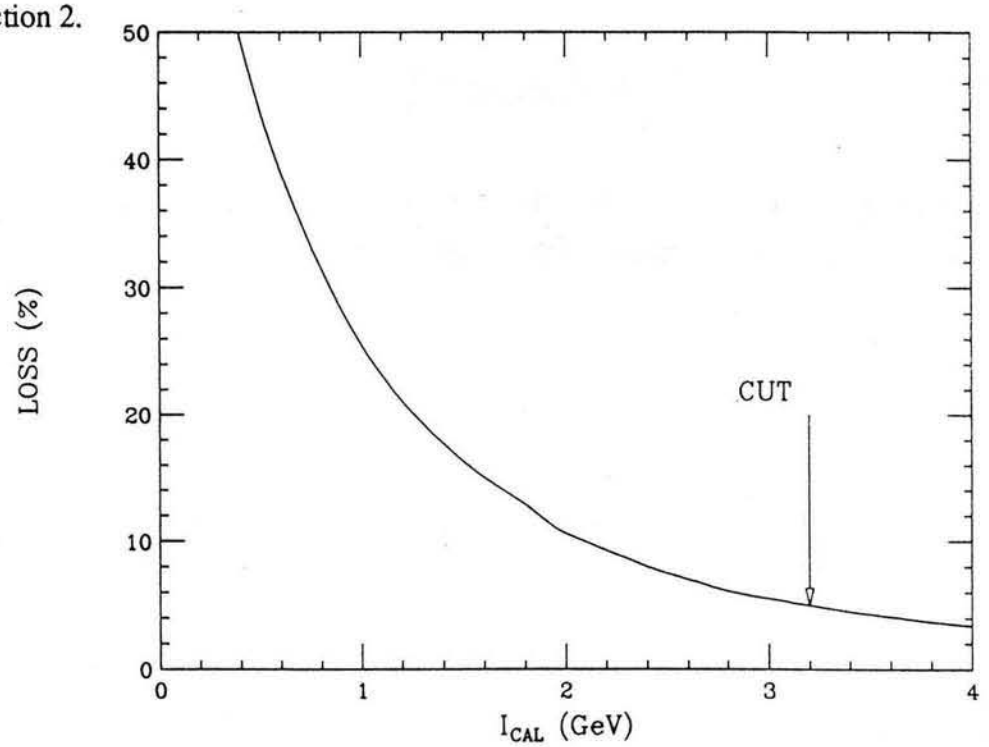

Fig. 10b: The loss of genuinely isolated track pairs as a function of the variable I_{CAL}.

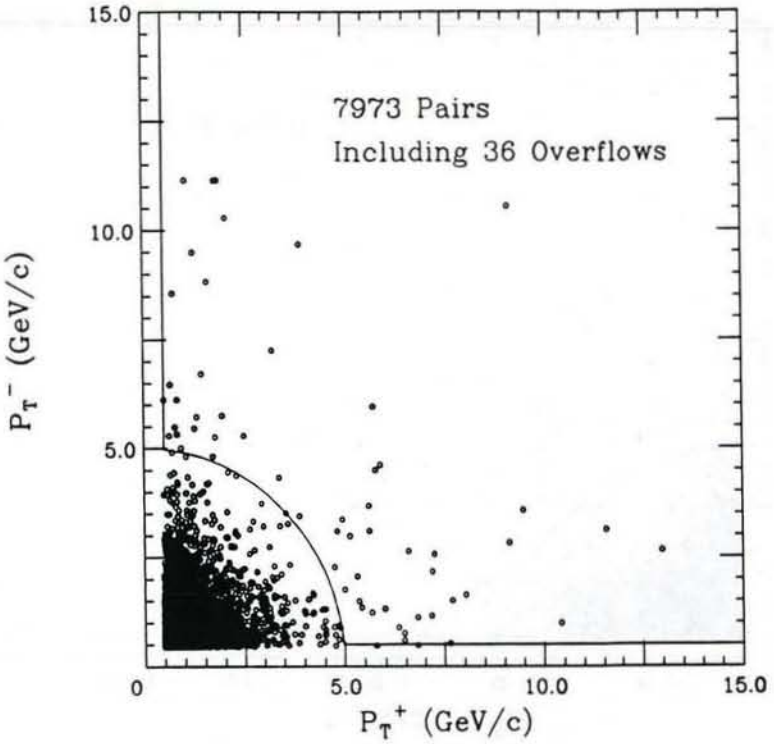

Fig. 11: Scatter plot of transverse momentum of positive tracks (p_T^+) versus transverse momentum of negative tracks (p_T^-) for pairs found in W/Z events satisfying the cuts listed in section 2. The solid lines indicate the cut at p_T = 500 MeV/c and $p_T^R > 5$ GeV/c.

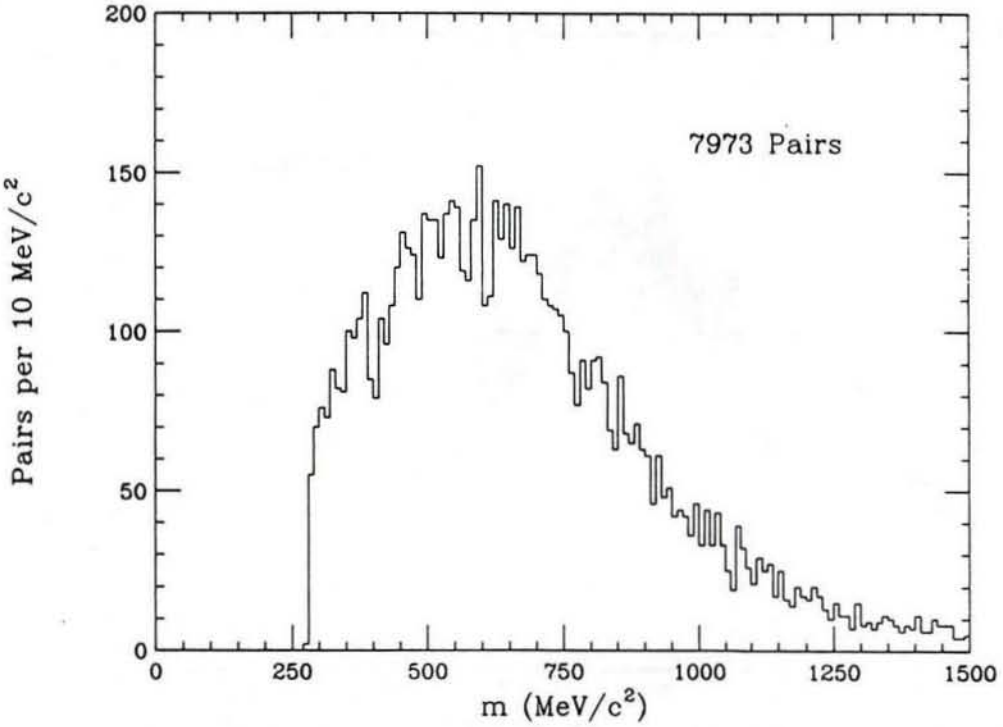

Fig. 12: The mass distribution for pairs treated as $\pi^+\pi^-$ found in W/Z events satisfying the cuts described in section 2.

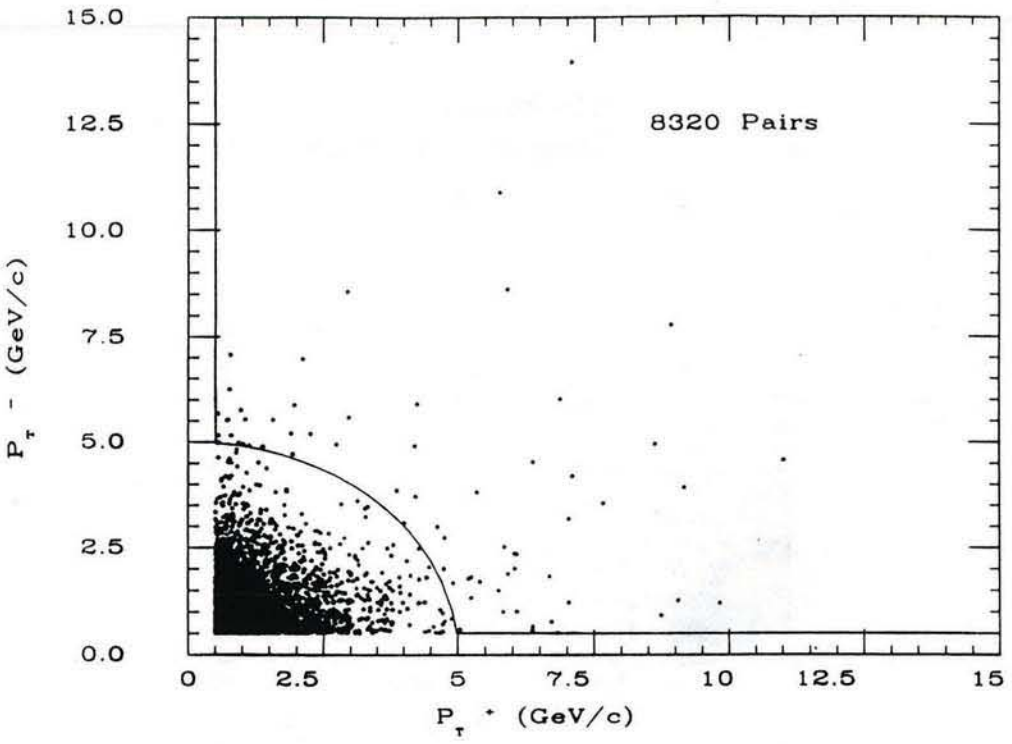

Fig. 13: Scatter plot of transverse momentum of positive tracks (p_T^+) versus transverse momentum of negative tracks (p_T^-) for pairs found in multijet events satisfying the cuts listed in section 2. The solid lines indicate the cut at p_T = 500 MeV/c and $p_T^R > 5$ GeV/c.

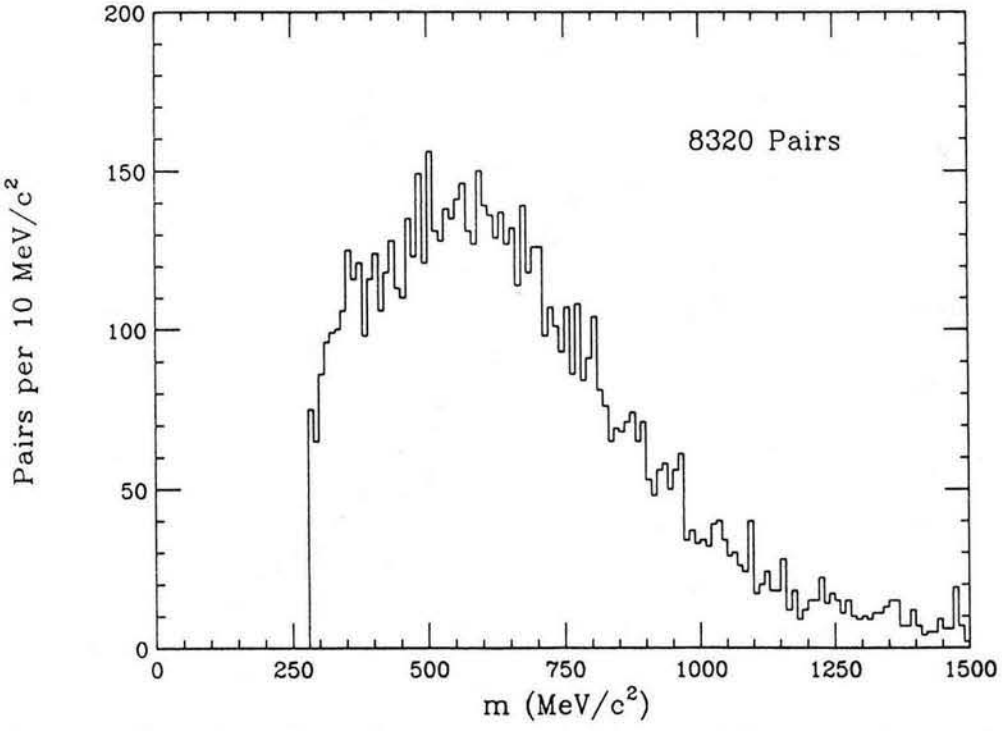

Fig. 14: The mass distibution for pairs treated as $\pi^+\pi^-$ found in multijet events satisfying the cuts described in section 2.

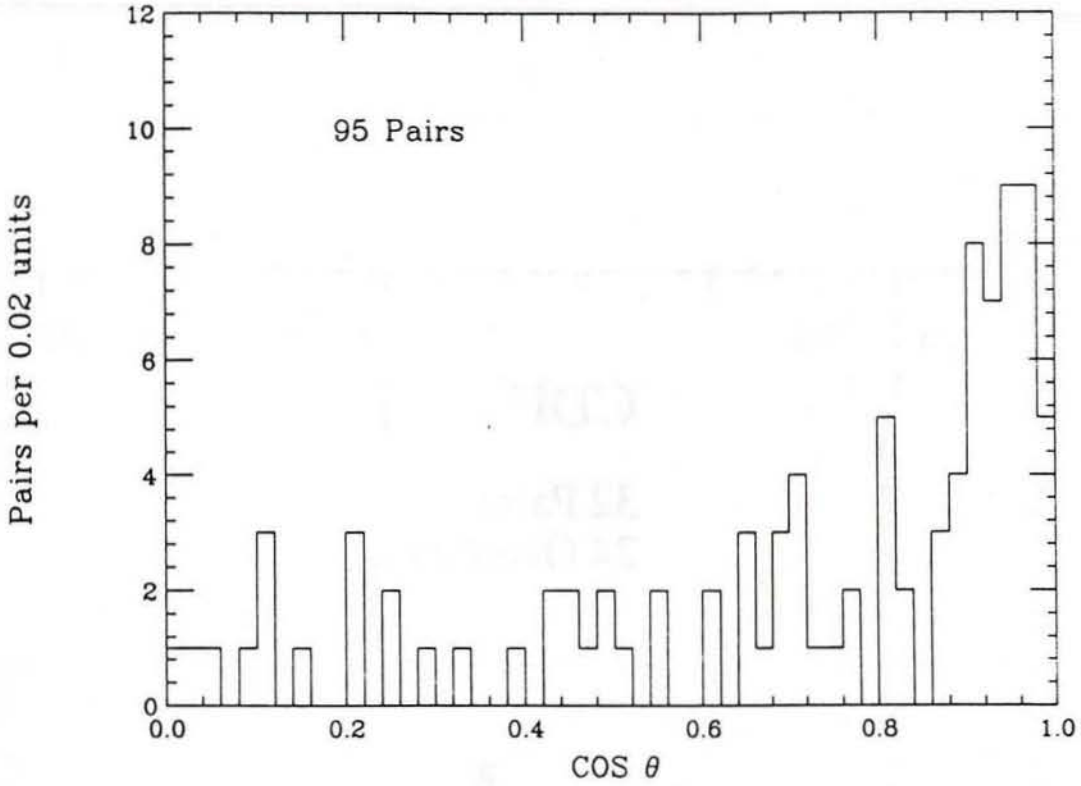

Fig. 15: The center-of-mass decay angular distribution (cos θ) for pairs found in W/Z events satisfying the cuts described in the text (before the cos θ cut).

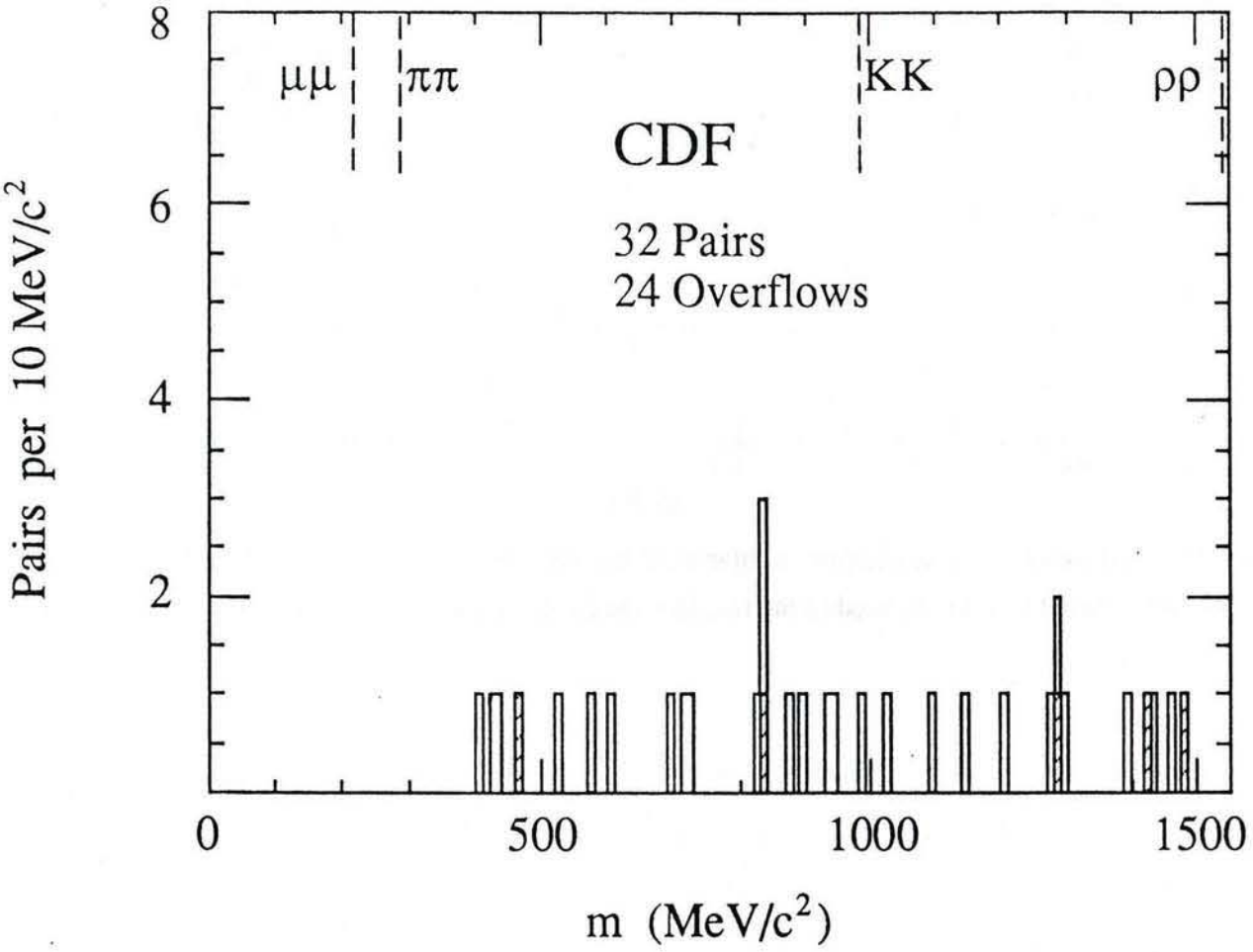

Fig. 16a: The final pair mass distribution in the mass region m < 1.5 GeV/c^2 after beam-constraint and track-refitting. The tracks have been assigned the pion mass. The μμ, ππ and KK thresholds are indicated by the vertical dashed lines. The data are plotted in bins of 10 MeV/c^2. (Note: the typical mass resolution in this region is 6.9 GeV/c^2.) The five hatched areas correspond to the events where the π/μ assignment for the tracks is ambiguous.

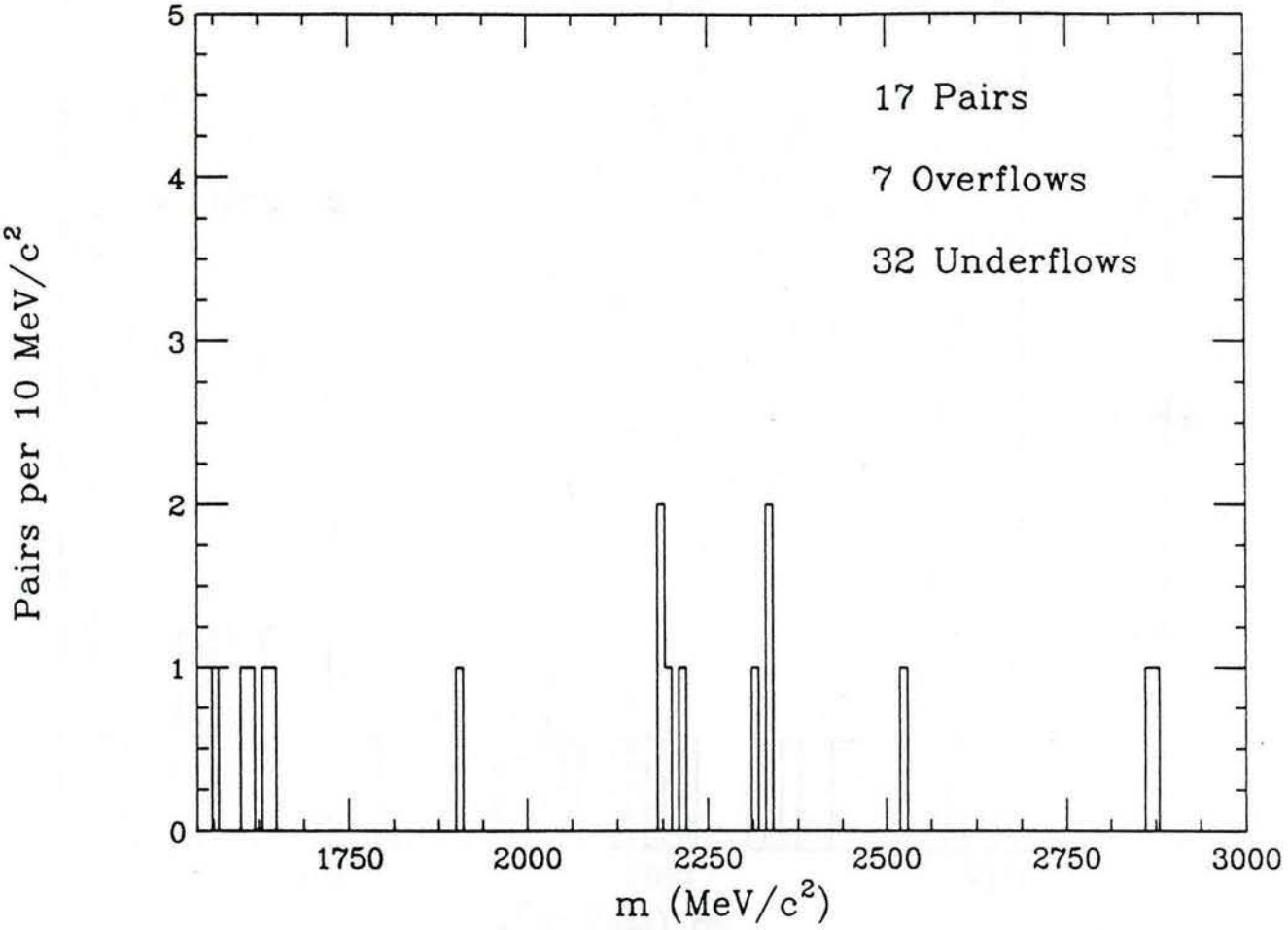

Fig. 16b: The final pair mass distribution in the mass interval $1.5 < m < 3.0$ GeV/c^2 after beam-constraint and track-refitting. The tracks have been assigned the pion mass.

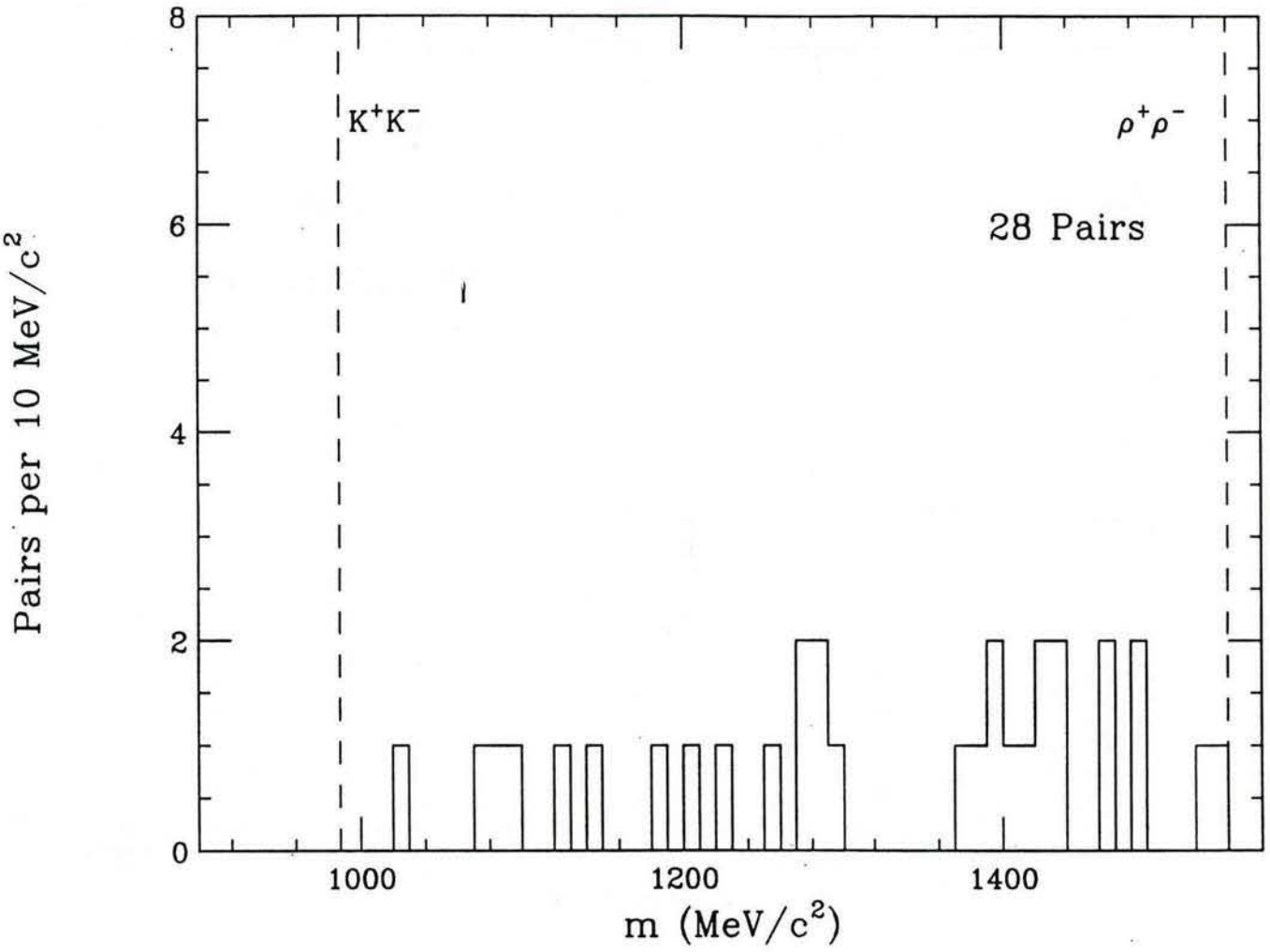

Fig. 16c: The final pair mass distribution in the mass interval $2m_K < m < 2m_\rho$ GeV/c^2 after beam-constraint and track-refitting. Both the $\pi^+\pi^-$ and the K^+K^- hypotheses are considered for the tracks.

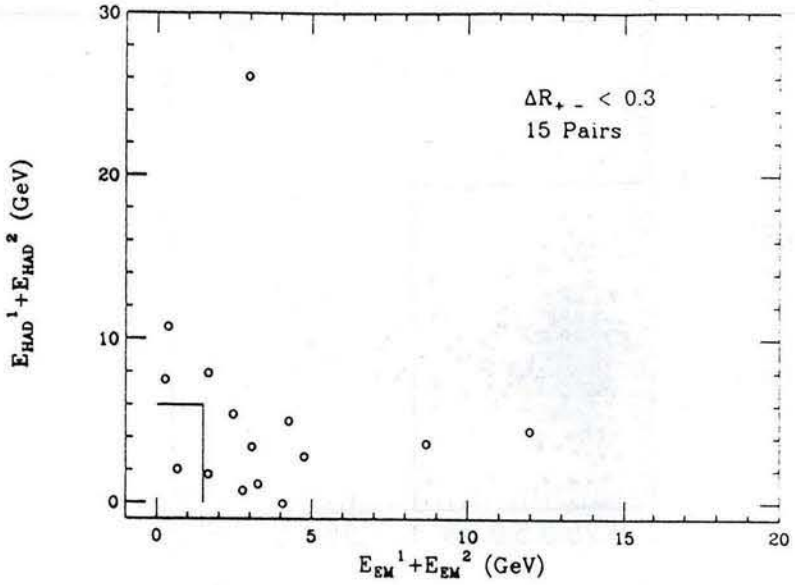

Fig. 17a: Scatter plot of the sum of the electromagnetic energy versus the hadronic energy deposited in the cells associated to the pair in the case where the separation ΔR_{+-} between the extrapolated tracks at the front face of the hadron calorimeter is less than 0.3. The solid lines indicate the boundary which divides those pairs that are assigned as pions from those where the assignment is ambiguous.

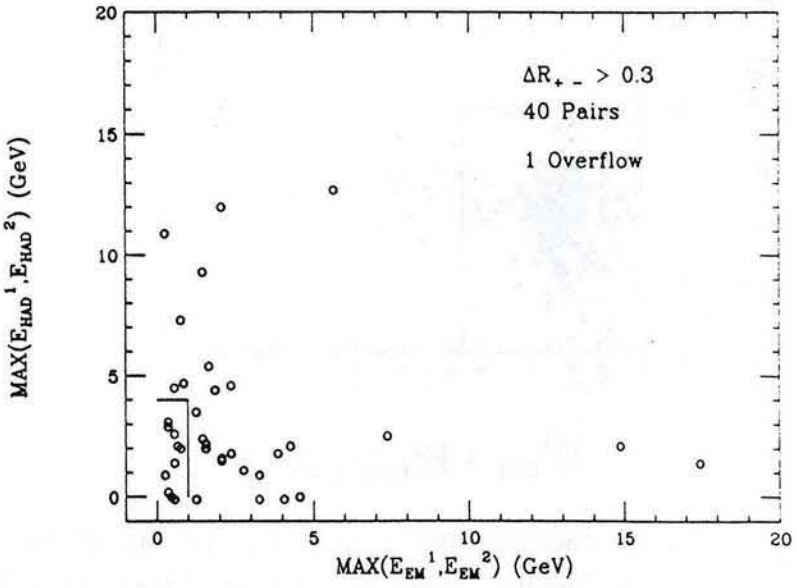

Fig. 17b: Scatter plot of the larger of the two electromagnetic energy depositions versus the larger of the two hadronic energy depositions in the cells associated to the pair in the case where the separation ΔR_{+-} between the extrapolated tracks at the front face of the hadron calorimeter is greater than 0.3. The solid lines indicate the boundary which divides those pairs that are assigned as pions from those where the assignment is ambiguous.

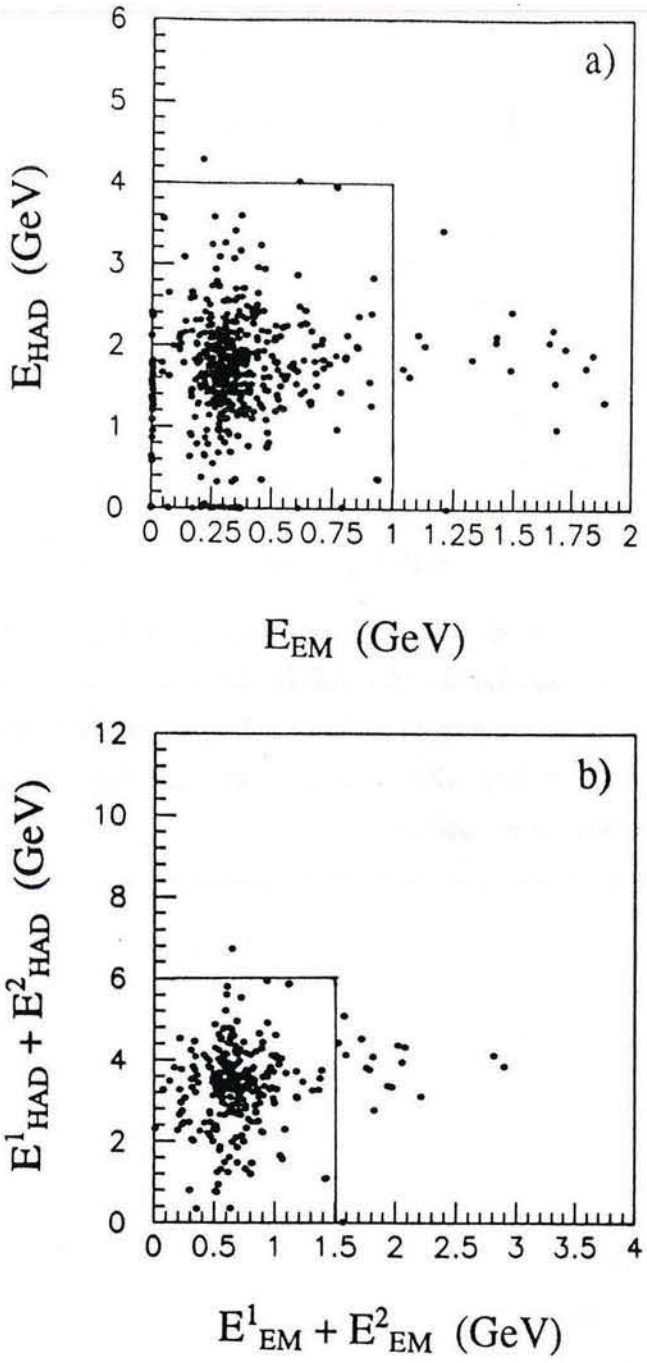

Fig. 18: **(a)** Scatter plot of the hadronic energy versus the electromagnetic energy for each leg in $J/\psi \rightarrow \mu^+\mu^-$ decays. The $\mu^+\mu^-$ hypothesis is rejected for tracks in the region outside the solid lines. **(b)** Scatter plot of the total hadronic energy versus the total electromagnetic energy for the two legs in $J/\psi \rightarrow \mu^+\mu^-$ decays. The $\mu^+\mu^-$ hypothesis is rejected for tracks in the region outside the solid lines.

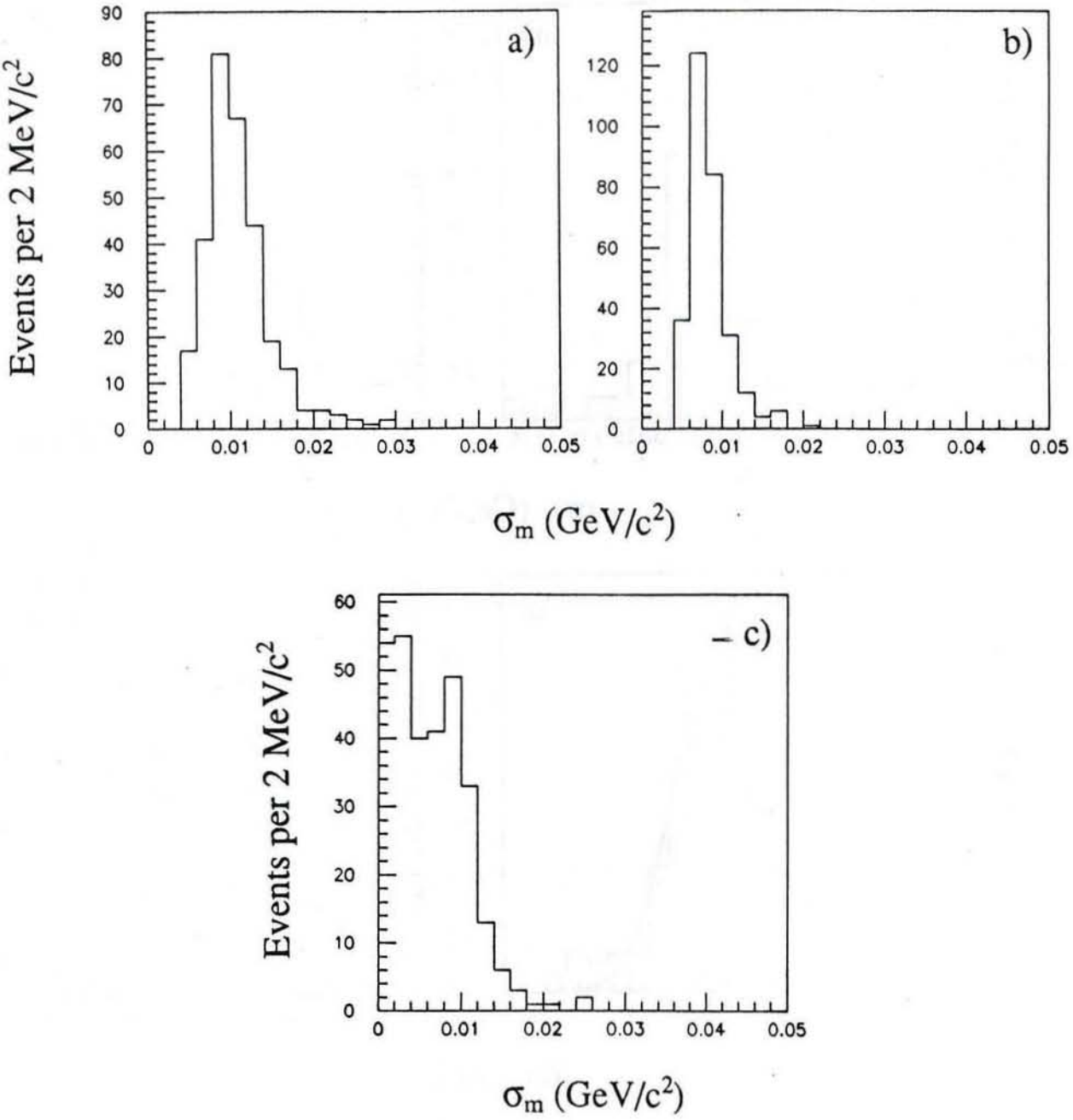

Fig. 19: The calculated mass resolution for ψ decays: **(a)** total, **(b)** the contribution from curvature and azimuth erros alone, and **(c)** the contribution from polar angle errors alone.

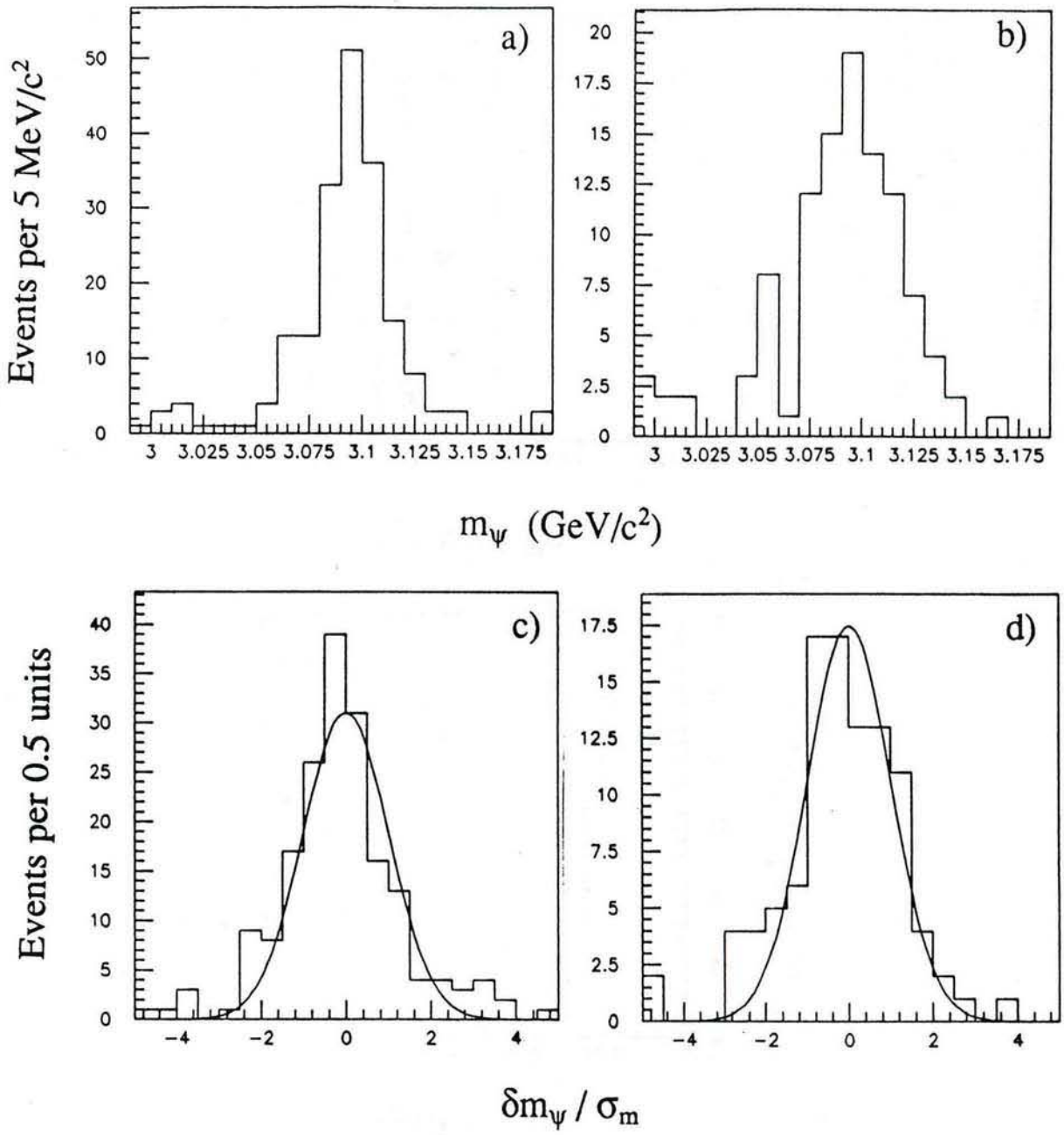

Fig. 20: The ψ mass for decays (**a**) in the case where δ(phi-curvature) is the dominant contribution to the mass resolution and (**b**) the case where δcot θ is the dominant contribution. In (**c**) the deviation from the ideal mass (δm) for the case where δ(phi-curvature) is the dominant contribution to the mass resolution and (**d**) for the case where δcot θ is the dominant contribution to the mass resolution has been normalized to the calculated mass resolution for each event, after including the degredation factor described in the text. The solid curves are unit width Gaussians with mean of zero.

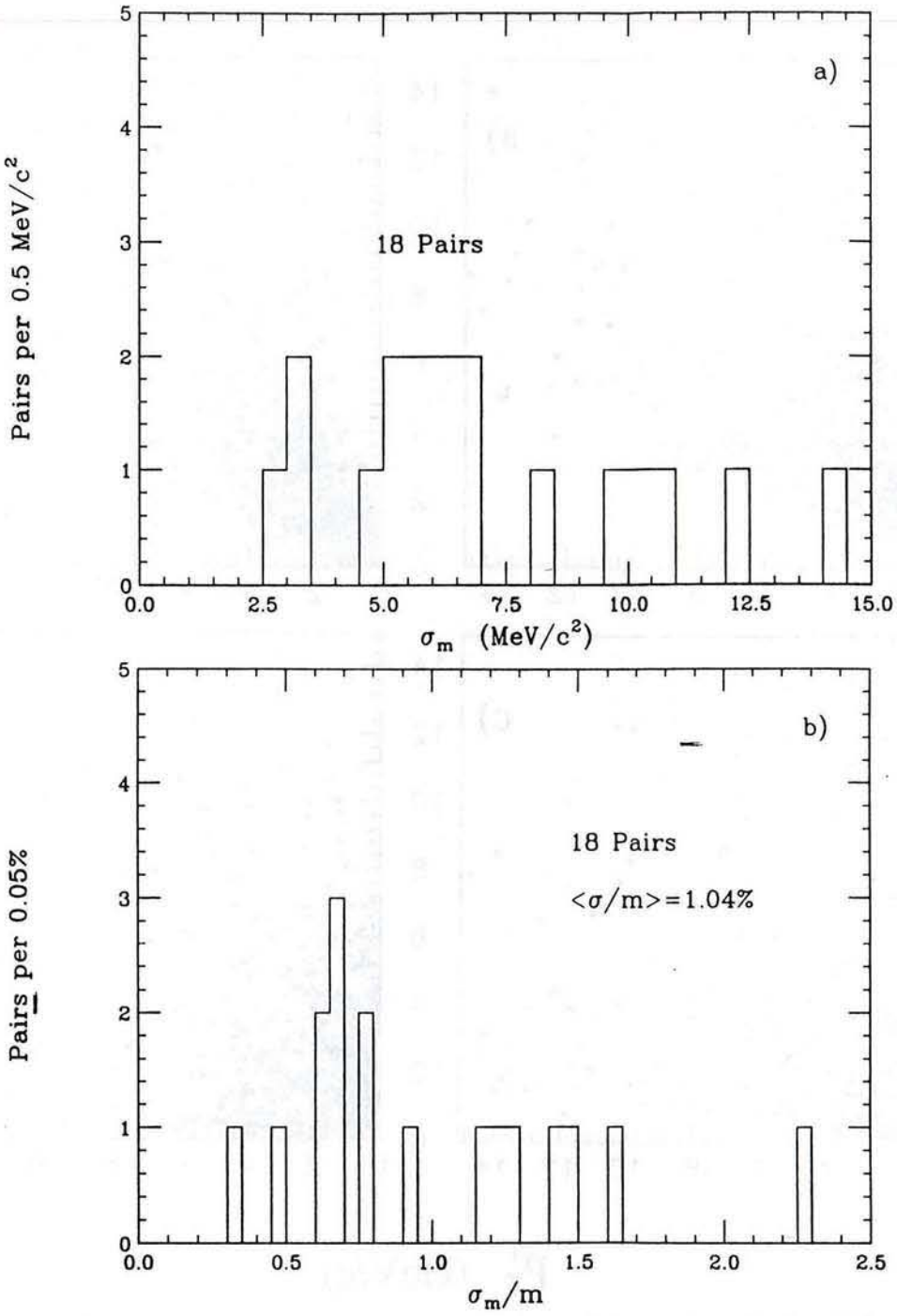

Fig. 21: The track pair mass resolution **(a)** σ_m and **(b)** σ_m/m calculated for events corresponding to the mass region plotted in fig. 15a and including the degredation factor discussed in the text.

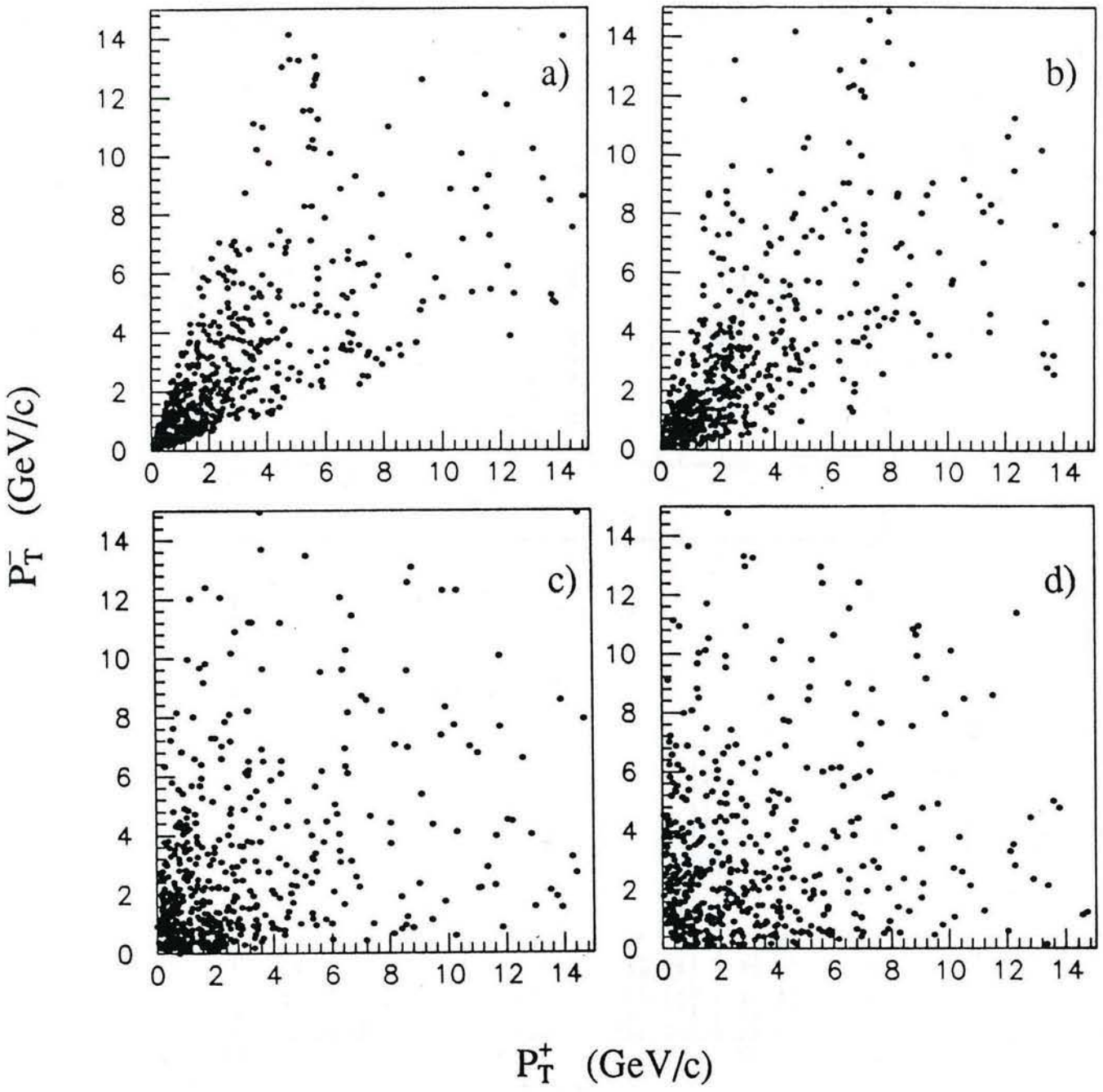

Fig. 22: Scatter plot of transverse momentum of positive tracks (p_T^+) versus transverse momentum of negative tracks (p_T^-) for the Higgs boson decay tracks satisfying the cuts listed in section 2 for m_H= **(a)** 250 MeV/c^2, **(b)** 350 MeV/c^2, **(c)** 500 MeV/c^2 and **(d)** 900 MeV/c^2. The shapes of the distributions at low mass are due to kinematics only.

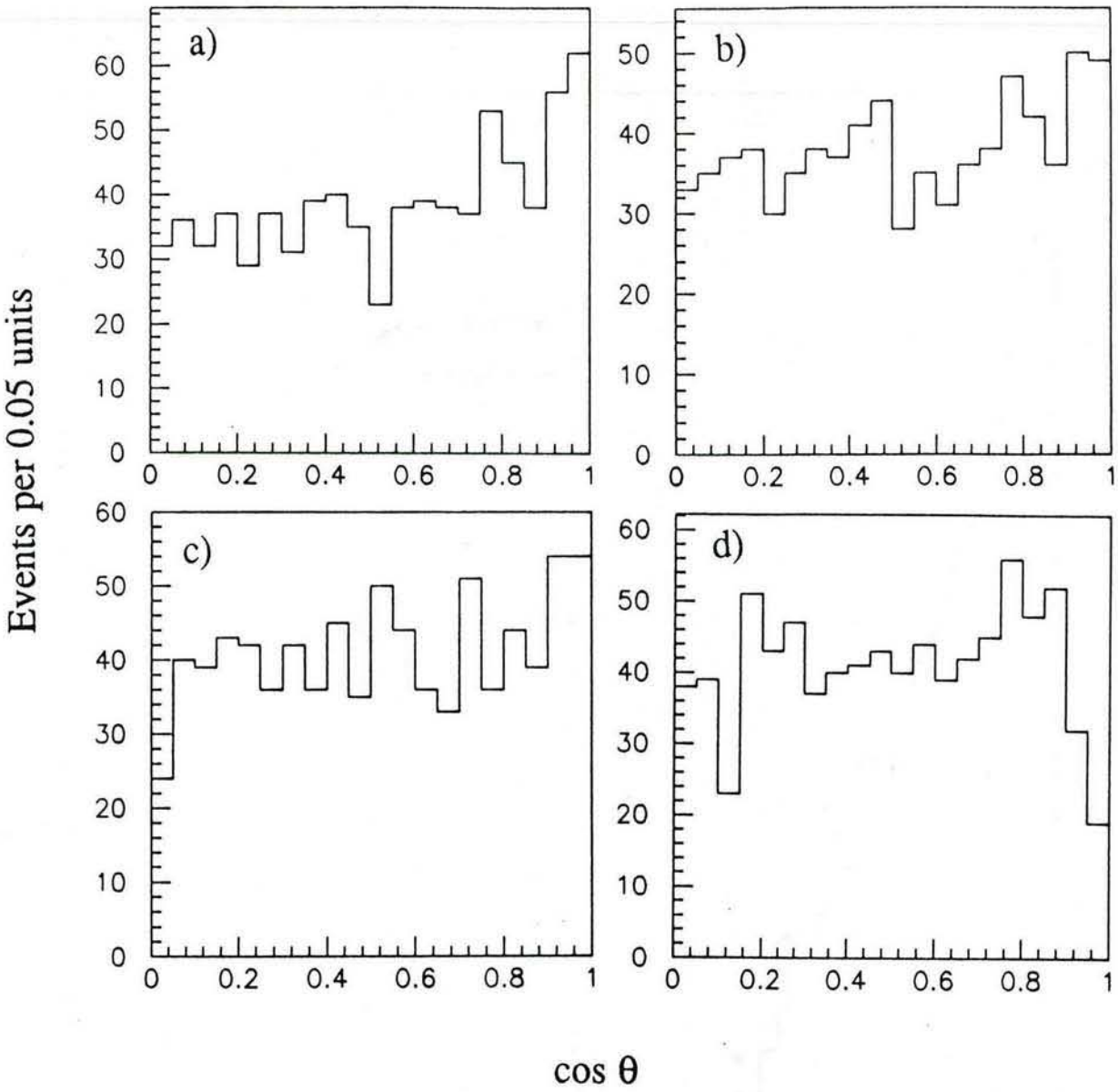

Fig. 23: The cos θ distributions for the Higgs boson decay tracks satisfying the cuts listed in section 2 for m_H= **(a)** 250 MeV/c^2, **(b)** 350 MeV/c^2, **(c)** 500 MeV/c^2 and **(d)** 900 MeV/c^2. The tracks have been assigned the pion mass. The forward peaking of the distribution in (a) is a consequence of assigning the pion mass to the tracks which are actually all muons. The depletion at large cos θ in (d) is a result of the transverse momentum cut at 500 MeV/c.

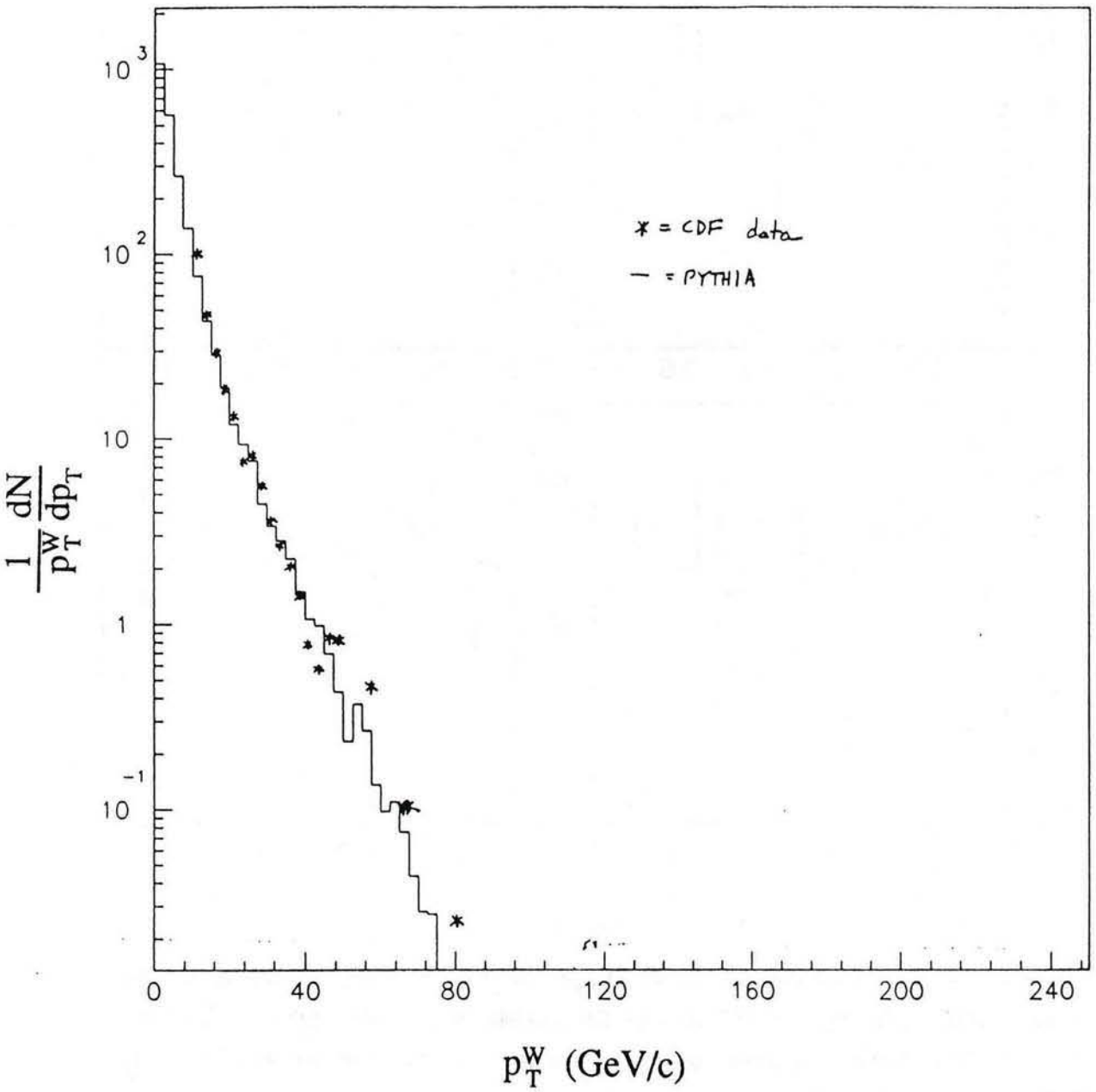

Fig. 24: Comparison of the observed W transverse momentum distribution with that from PYTHIA, after smearing the parton level energies by $15\%/\sqrt{E}$ and the neutrino energy by $0.7/\sqrt{30+p_T^W}$ to allow for detector resolution.

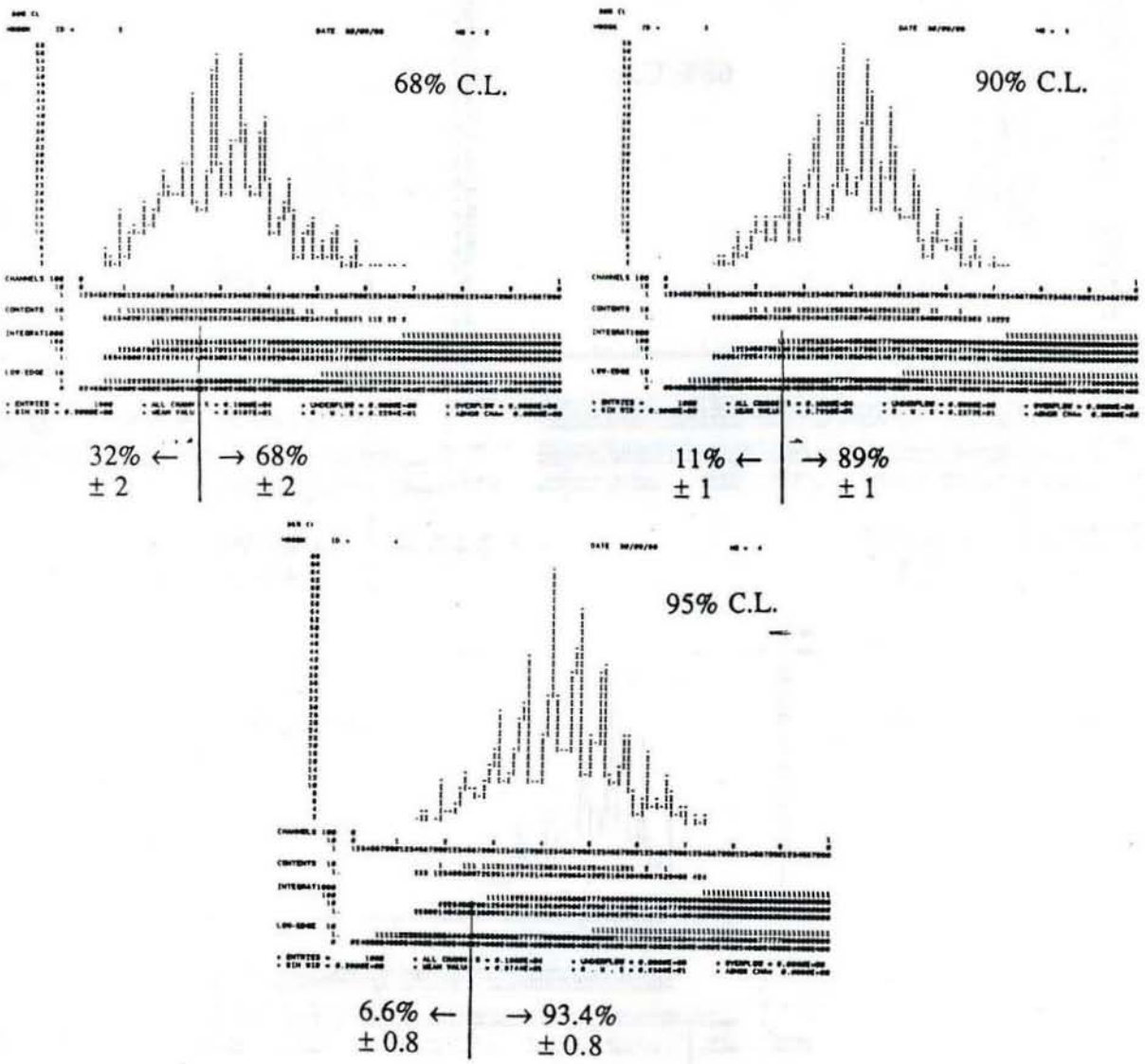

Fig. 25a: Distribution of 68%, 90% and 95% upper confidence limits found by the fitting program for 1000 generated experiments in which the mean number of Higgs bosons = 5.

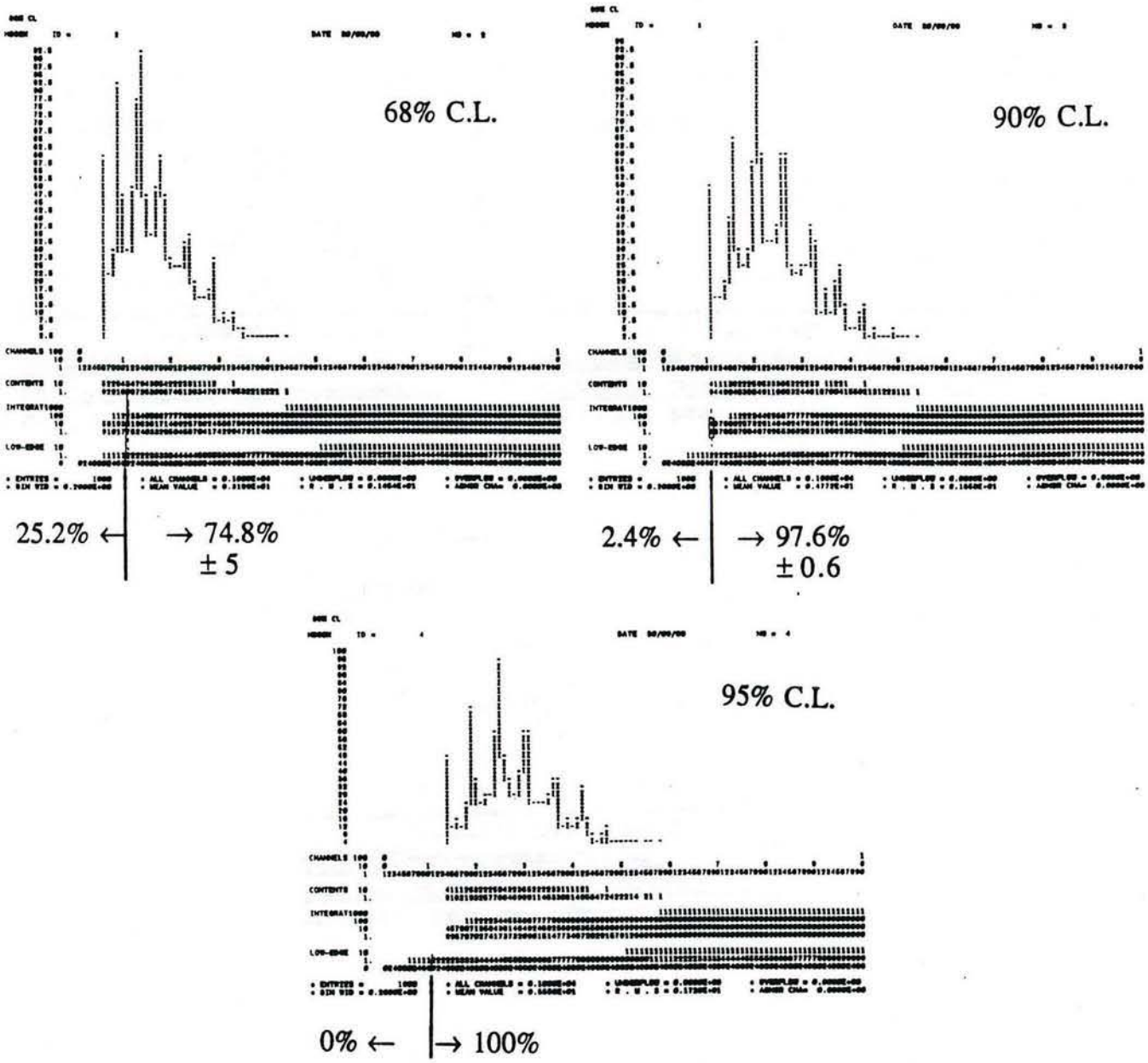

Fig. 25b: Distribution of 68%, 90% and 95% upper confidence limits found by the fitting program for 1000 generated experiments in which the mean number of Higgs bosons = 2.

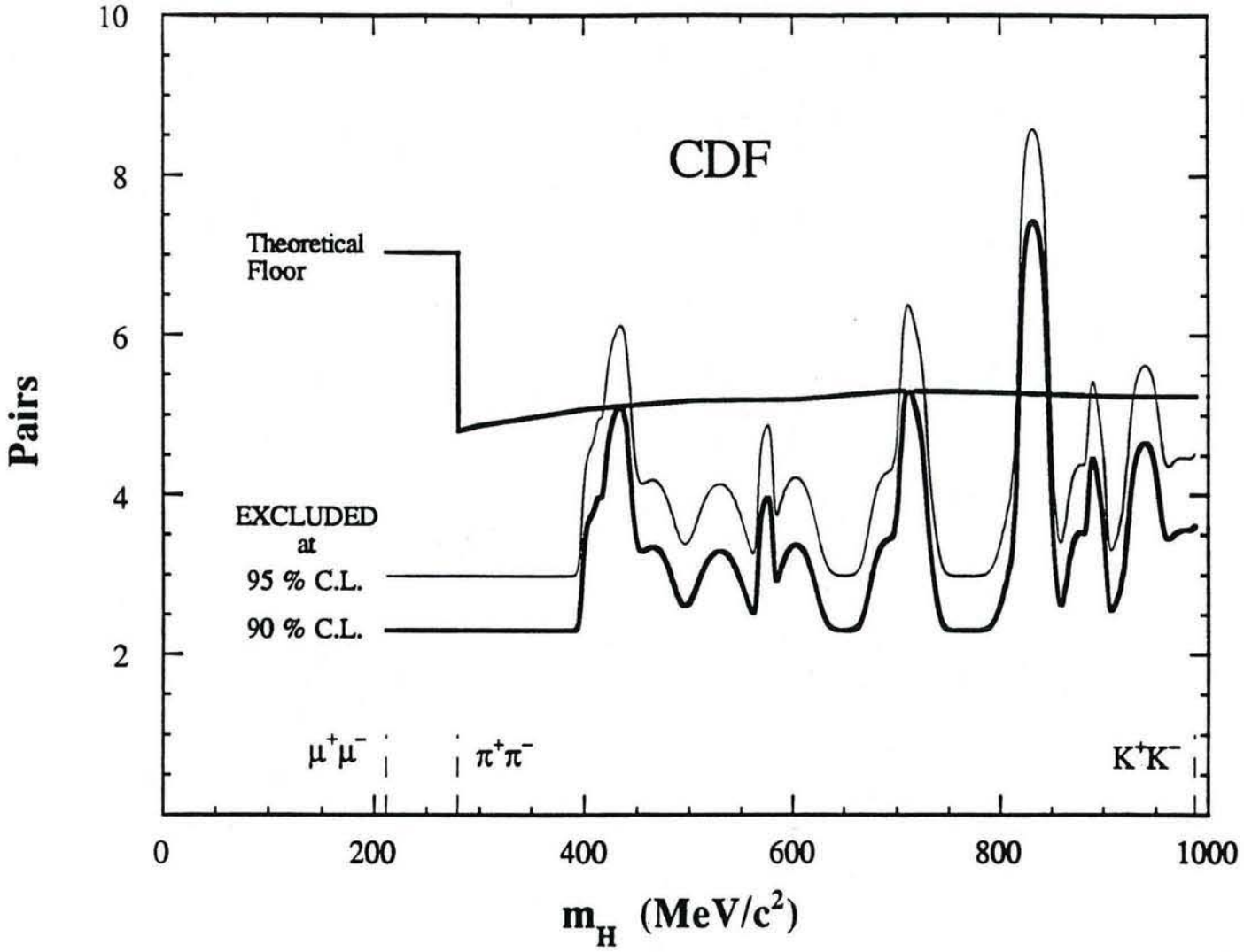

Fig. 26: Theoretical floor on the predicted number of Higgs bosons surviving our selection criteria shown as a function of pair mass and compared with the 90% and 95% upper confidence limit on narrow resonance production of track-pairs in the selected samples .